Calibration of the HRC-S UV/Ion Shields

# 1 Introduction

The x-ray transmission characterisitics of the flight HRC-S UV/Ion shield (S/N-002) are based on measurements carried out at both the SAO's HRC laboratory and at the Physikalish-Technische Bundensanstalt (PTB) radiometry laboratory of the BESSY 1 synchrotron in Berlin, Germany. The measurements were made using the witness samples delivered along with the flight filter, which was manufactured by the Luxel Corporation of Friday Harbor, WA. Luxel physically measures the thickness of their foils with a high-quality profilometer manufactured by Tencor. Its mechanical stylus measures the step height across an edge in the material with a resolution of $\pm 5\mathring{A}$. When calibrated against a known standard, it has been their experience that it performs within the uncertainty of the standard, which is $\pm 17\mathring{A}$. We have found that Luxel's aluminum and polyimide thickness measurements agree with our derived thickness measurements of the constituent filter layers, within the statistical uncertainties.

A given pair of witness samples comes from the same filter production run as the associated segment of the flight filter, and are taken from different regions of the larger filter sheet. We measured witness samples representing the HRC-S UV/Ion shield (UVIS-S) $\pm 1$ segments (both thin and thick aluminum regions) as well as the thick aluminum region of the central filter segment. A witness sample of the central segment's thin aluminum region was not available for testing. Those transmission measurements that were carried out on identical witness samples at both facilities yielded statistically similar fits. We used this fact in developing our x-ray transmission models of the various segments of the UVIS-S. Figure 1 shows the nominal thickness values of the constituent layers of the UVIS-S. A detailed account of our measurements was presented at the 1997 SPIE conference in San Diego, CA.[1] This report can be accessed through the HRC calibration web site at

http://hea-www.harvard.edu/HRC/calib/spie97.html.

## 1.1 SAO and BESSY Instrumental Setups

The SAO measurements to characterize the flight UVIS-S x-ray transmission were carried out on the witness samples (see table 1) using a McPherson model 248/310 G 1-meter diameter grazing incidence monochromator. It is equipped with a 1200 G/mm grating that has a $2^o5'$ blaze angle and a $5442\mathring{A}$ blaze wavelength, which yields an operating range of 2.8 $\mathring{A}$ to 340.7 $\mathring{A}$. The monochromator entrance and exit slits were set to a nominal 20 $\mu$m width to minimize contamination by the x-ray continuum. Figure 2 represents a typical monochromator beam scan to identify the fluorescent lines associated with the anode selected for use in the Manson model 2 single-anode soft x-ray source. In this case, the anode is titanium. The scan shows that the Ti $L_\alpha$ and $L_\eta$ lines dominate over the continuum by about a factor of 10.

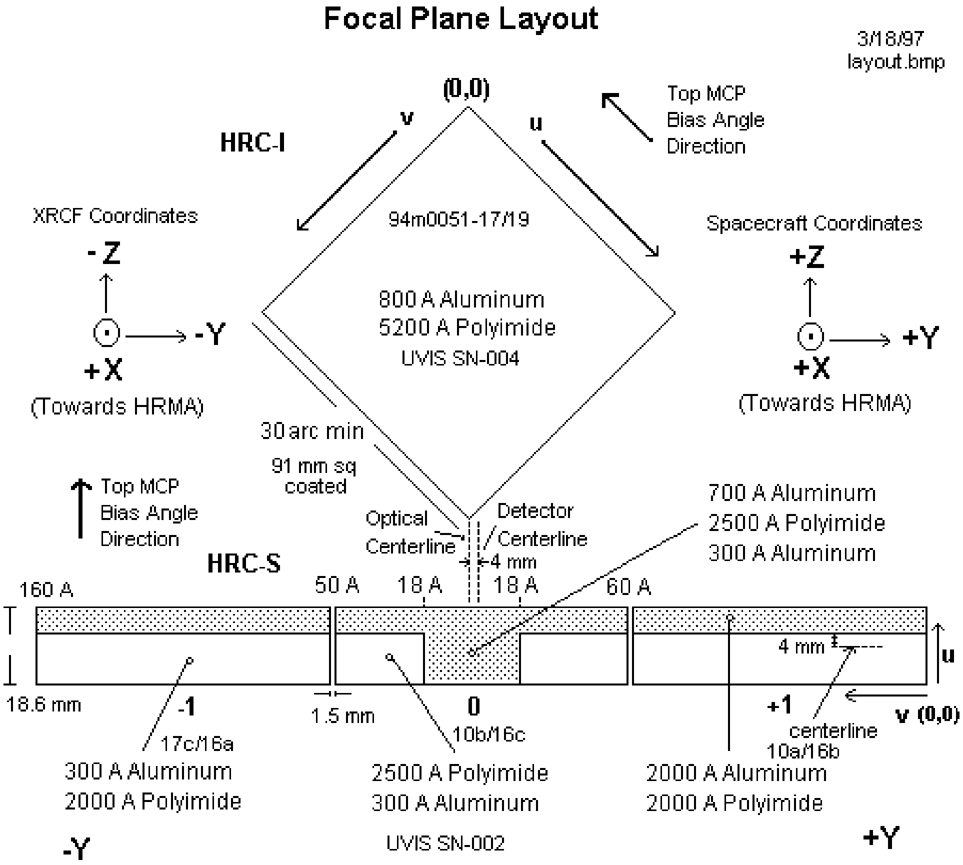


Figure 1: The material composition of the UVIS-I and UVIS-S are shown above. The thicknesses are nominal. Where there is only a single side coated with aluminum, that side faces the High Resolution Mirror Assembly (HRMA) of Chandra. For the HRC-S Inner "T", it is the side with the 700Å coating that faces the HRMA. The figure also shows the relative orientation of the HRC-I and HRC-S in the instrument focal plane.

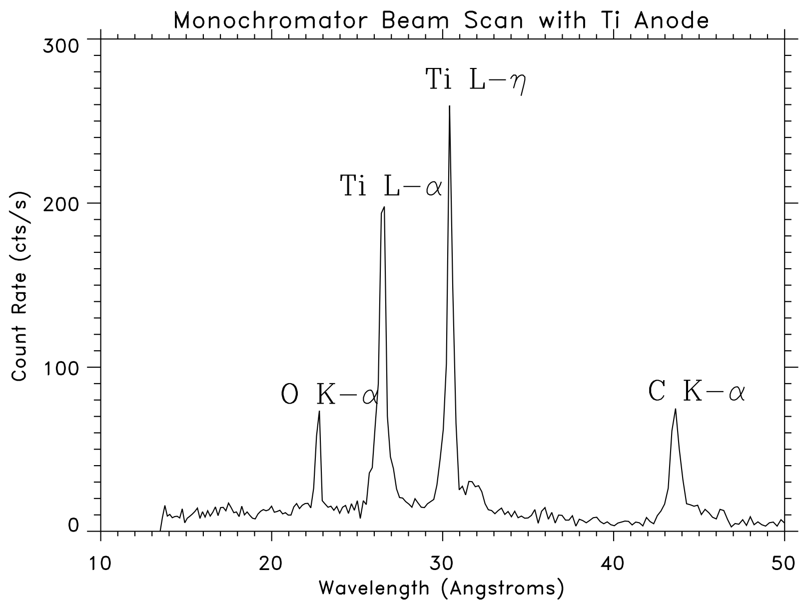


Figure 2: Example of a typical monochromator beam scan to identify the first order x-ray fluorescent lines associated with an anode. In this case, titanium. Note how the primary lines of interest, Ti $L_\alpha$ and $L_\eta$, dominate over the continuum.

When a fluorescent line is selected, the monochromator is adjusted to operate at its peak. The instrument is also equipped with a pair of filter wheels, each of which has enough holders to accomodate up to five witness samples. However, one holder of each wheel was intentionally left unoccupied so that x-ray spectra could be obtained without a filter in the x-ray detector beam path as part of the transmission measurement procedure. Spectra were acquired with a Manson model 851 gas-flow proportional counter equipped with a VYNS window, and which utilized methane as the fill gas.

The SAO experimental setup precluded any effort to perform spatial uniformity measurements on a given witness sample. Rather, each measurement represents an average transmission over a filter. However, we know from previous uniformity measurements of a flight candidate HRC-I UV/ion shield, that it was spatially uniform in transmission within 5% relative error at a spatial scale of 1 mm.[2]

The BESSY synchrotron measurements were conducted at station 11.31 of the Physikalish-Technische Bundensanstalt (PTB) radiometry laboratory. With this facility, it was possible to measure the x-ray transmission in the absorption edge fine structure regions. These occur at the Al L-edge, as well as at the K-edges of carbon, nitrogen, oxygen and aluminum. The beam-line of the facility includes an SX-700 type plane grating monochromator with a useful photon energy range of 60 - 2000 eV and spectral resolution ranging from $E/\Delta E = 2500$ at 100 eV to $E/\Delta E = 700$ at the Al-K edge. A test chamber (700 mm long, 600 mm in diameter) was provided with a vacuum-compatible micro-positioning system for the manipulation of witness samples and detectors. Two detectors were used: a GaP/Au Schottky-type photodiode (Hamamatsu G1963) with a sensitive area of 4.6 mm$\times$4.6 mm; and a VALVO X913 BL channel electron multiplier (CEM). The photodiode performs well and is actually used at all surveyed energies with the exception of the 283-300 eV range, where the CEM is more appropriate because of the low flux available in that region.

The witness samples were mounted on a four-position fixture (one position left open) attached to a micro-positioning system allowing complete two dimensional scans of the sample. A 400 $\mu$m spot size was chosen as the best compromise between flux stability and spatial resolution. Table 2 describes the energy scans in detail.

Each individual measurement at a given energy is the average of 3 independent consecutive detector readings. If the readings are not consistent with each other to within 1%, the measurement is automatically repeated. Each measurement is normalized by the current of the beam in the storage ring. This procedure accounts for the time dependence of the beam, ensuring measurement stability at the 1% level over a time scale of 30 minutes. In order to ensure no significant drift between measurements at the open and sample positions, all of our measurement sets were taken over time scales shorter than 10 minutes.

The measurement technique described above ensures a statistical uncertainty within 1% at all energies. Stray light contribution in the monochromatic radiation between 1.0 and 1.7 keV is up to 2%, resulting in a transmission uncertainty within 1% for measured samples like ours. Above 1.7 keV, the stray light contamination is higher, and results in a measurement uncertainty up to 3%. Second order contamination is particularly significant at low energies ( $E < 130$ eV), and in a small region above the carbon edge (290-300 eV), resulting in a measurement uncertainty of up to 30%. Outside of these regions, the measurement uncertainties are always lower than 3%.

### 1.2 Modeling the X-ray Transmission

Each transmission model is a synthesis of the SAO and BESSY models as derived from the measurements. For energies at and below 1950 eV, the x-ray transmission is represented by the model derived from the BESSY data. Above 1950 eV, the transmission curve is based upon the mass areal densities derived from the SAO monochromator measurements. We are justified in taking this approach because the BESSY and SAO fits are statistically similar outside of the fine structure regions. Figure 3 shows this to be the case. It is a plot of the SAO and BESSY x-ray transmission models in the thick aluminum region of the central filter segment. Superimposed on the models are the x-ray transmission measurement results obtained of the associated witness sample for this segment using the SAO x-ray monochromator. For each UV/Ion shield, the SAO and BESSY derived models match up very well at 1950 eV.

Modeling of the synchrotron data was a two step process. We first applied a nonlinear fitting routine (the Levenberg-Marquardt algorithm) to each witness sample data set, to the exclusion of the absorption edge fine structure regions. The transmission of x-rays through N layers of material is represented by

$$T(E) = \prod_{i=1}^{N} e^{-(\frac{\mu(E)}{\rho})_i (\rho t)_i} \tag{1}$$

where the product of the material density and thickness, $\rho$ and t, respectively, is called the mass areal density. In fitting a model to the data, the mass areal densities of Al, C, N and O were adjusted in such a way as to minimize the reduced $\chi^2$ value of the fit. This same technique was applied to the SAO monochromator data sets.

From the derived mass areal densities, and the canonical densities of aluminum ($2.50\ g \cdot cm^{-3}$) and polyimide ($1.40\ g \cdot cm^{-3}$), one can determine the thickness of the constituent layers of the filter. Therefore, the x-ray transmission model for the UVIS-S can also be expressed as

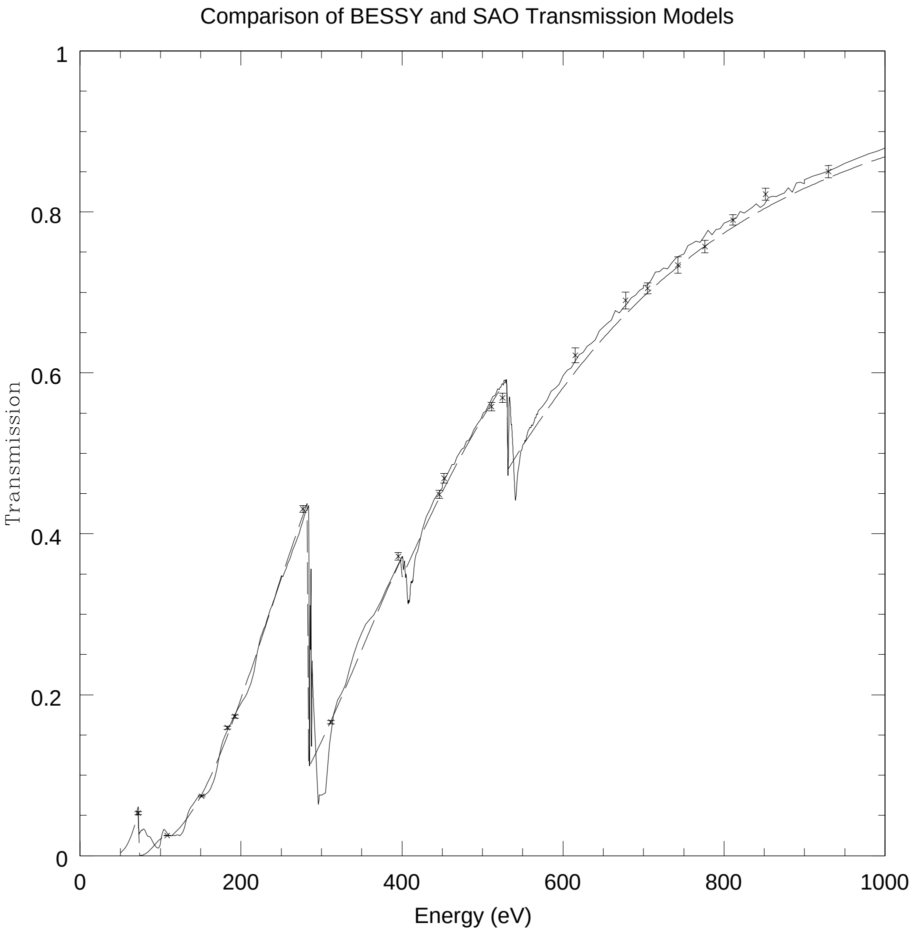


Figure 3: This plot demonstrates that, outside of the fine structure regions, we obtained statistically similar fits to transmission data of witness samples measured at both SAO (dashed line) and the BESSY facility (solid line). Superimposed on the model plots are the SAO x-ray transmission measurement points of the witness sample representing the central filter segment in the thick aluminum region.

$$T(E) = e^{-(\frac{\mu(E)}{\rho})_{Al}\rho_{Al}t_{Al}} e^{-(\frac{\mu(E)}{\rho})_{polym}\rho_{polym}t_{polym}} \tag{2}$$

The mass absorption coefficients are taken from Henke, *et al*, (1982). These coefficients provide the best statistical fit to our data.

The mass attenuation coefficients derived for a compound by taking into account only the individual atomic coefficients does not take into consideration fine structure features that occur near the absorption edges due to interactions of the photoelectrons with the closer atoms in the molecules of the compound (XANES and EXAFS). In order to define the mass attenuation coefficients of a compound that include these features, direct transmission measurements need to be conducted on the compound material of interest. Following the same technique described by us in an earlier work[3], we used the synchrotron measurements and the best fit model parameters of the witness sample with the thickest layer of polyimide (a flight witness sample for the HRC-I UV/Ion shield) to derive the mass attenuation coefficients of C, N, and O near their K absorption edges. Analogously, we used the measurements and the best fit model parameters of the witness sample with the thickest layer of aluminum (a flight witness sample for the HRC-S UV/Ion shield's -1 segment in the thick aluminum region) to derive the mass attenuation coefficients of Al near its K and L absorption edges. This approach works well except at the carbon fine structure region, where higher order ($3^{rd}$ order and higher) contamination yields an unsatisfactory fit.

## 1.3 Modeling Results

The results of fitting the SAO monochromator data to the flight UVIS-S witness samples are shown in table 3. This gives the mass areal densities for the constituent elements based on the 1982 Henke mass absorption coefficients. From these fits we were able to derive the thickness of the aluminum layer of each filter. We show this in table 4. It shows that our derived aluminum thickness values agree with Luxel's, within the statistical uncertainties. In table 5 we show the polyimide thickness values derived from the SAO data. Luxel's measurements are shown for comparison. Table 6 compares the BESSY and SAO best fit results for the $\pm 1$ segments in differing aluminum thickness regions. For a given segment, the BESSY and SAO best fit results for the constituent elements of polyimide agree within the statistical uncertainties. By taking the ratio of the aluminum mass areal densities of a given pair of segments in table 6, one obtains results that are consistent with the ratio of Luxel's aluminum thickness measurements. This fact is brought out in table 7.

There are no witness samples for the thin aluminum region of the central segment of the UVIS-S. The transmission of this region was determined by dividing the measured transmission of a witness sample representing the thick aluminum region of the central segment by the calculated transmission of the difference in thickness of aluminum (provided by the manufacturer) between the two regions. We have found that, in general, the nominal aluminum thicknesses of the shields as measured by Luxel agree well with our measurements of the areal densities. The transmission of the thin aluminum region was computed using: the difference in nominal aluminum thickness of the central segment; the nominal density of deposited aluminum ($2.5\ g \cdot cm^{-3}$); the 1982 Henke coefficients; and the measured transmission of the shield in the region of thick aluminum.

This procedure works well above 200 eV. However, the measured jump ratio across the Al L-edge at 72.4 eV of the witness sample representing the thick aluminum region of the central segment is considerably less (i.e., the transmission is greater) than what one would predict based on the Henke absorption coefficients and the nominal aluminum thickness. Therefore, our model which uses these absorption coefficients over-estimates the absorption of the difference in aluminum, and the computed transmission of the thin region becomes unphysical (i.e., $> 1$). A slightly more complex procedure had to be used.

The areal densities of the other constituents of the shield (i.e., C, N, and O) are known from the fitting. From the measured x-ray transmission of the witness sample representing the thick aluminum region of the central segment and the mass absorption coefficients of C, N, and O, one can compute an 'effective' mass absorption coefficient for aluminum as a function of energy. Above 200 eV, there is little difference between this effective mass absorption coefficient and the tabulated value. Below 200 eV, however, the effective mass absorption coefficient is considerably less than the tabulated value. Using this new set of absorption coefficients for aluminum, the transmission of the thin aluminum region of the UVIS-S central segment can be computed. The transmission versus energy is shown in figure 4 with a more detailed plot below 2keV shown in figure 5. The transmission in the K-edge fine structure regions of this filter is shown in figures 6 through 9.

The transmission of the thick aluminum region of the central segment of the UVIS-S is shown in figure 10 with a more detailed plot below 2keV shown in figure 11. Figures 12 and 13 are similar to figure 11, though they include the SAO and BESSY data, respectively. We derived a polyimide thickness of $2750 \pm 118 Å$ and an aluminum thickness of $952.8 \pm 18.0 Å$ based on the modeling of the SAO monochromator data. The modeled transmission in the K-edge fine structure regions of this filter are shown in detail in figures 14 through 17, along with the BESSY data obtained on a representative witness sample.

The transmission of the thick aluminum region of the $\pm 1$ segments of the UVIS-S is represented by figure

18 with a more detailed plot below 2keV shown in figure 19. This model is based in part on the synchrotron measurements of the $-1$ segment. Synchrotron measurements of a witness sample representing the thick aluminum region of the $+1$ segment were not obtained. However, the $+1$ and $-1$ segment measurements in the thick Al region obtained on witness samples with the SAO monochromator yielded statistically similar fits. Figures 20 and 21 are similar to figure 19, though they include the SAO and BESSY data, respectively. We derived a polyimide thickness of $2120 \pm 140\mathring{A}$ and an aluminum thickness of $1980 \pm 35\mathring{A}$ based on the modeling of the SAO monochromator data. The modeled transmission in the K-edge fine structure regions of this filter are shown in detail in figures 22 through 25, along with the BESSY data.

The transmission of the thin aluminum region of the $\pm 1$ segments of the UVIS-S is represented by figure 26 with a more detailed plot below 2keV shown in figure 27. Figures 28 and 29 are similar to figure 27, though they include the SAO and BESSY data, respectively. Because synchrotron measurements of witness samples in the thin Al region of the $-1$ segment were not obtained, the transmission was calculated from measurements of the witness sample representing the thick aluminum region of the $-1$ segment, the known mass absorption coefficients, and the aluminum thicknesses (both thin and thick regions) as provided by Luxel. The modeled transmission in the K-edge fine structure regions of this filter are shown in detail in figures 30 through 33, along with the BESSY data points obtained from measurements made of the thin Al region of the $+1$ segment. Based on the SAO monochromator data, we derived an aluminum thickness of $316 \pm 19\mathring{A}$. The polyimide thickness is the same as above, $2120 \pm 140\mathring{A}$.

# 2 References


1. G.R. Meehan, S.S. Murray, M.V. Zombeck, R.P. Kraft, K. Kobayashi, J.H. Chappell, A.T. Kenter, M. Barbera, A. Collura, S. Serio, "Calibration of the UV/Ion Shields for the AXAF High Resolution Camera," Proc. SPIE, 3114, 1997

2. G.R. Meehan, A.T. Kenter, R.P. Kraft, S.S. Murray, M.V. Zombeck, K. Kobayashi, J.H. Chappell, M. Barbera, and A. Collura, "Measurement of the transmission of the UV/Ion Shields for the AXAF High Resolution Camera," Proc. SPIE, 2808, 1996.

3. Barbera, M., Collura, A., Dara, A., "Calibration of the AXAF-HRC UV/Ion shields at Osservatorio Astronomico di Palermo G.S. Vaiana: III - Synchrotron measurements of XANES in aluminum coated Lexan film samples," 1996, SPIE vol. 2808, 120.

# 3 Tables and Figures

| Flight Filter Segment | Composition and Luxel Thickness Measurements | Test Method |
|---|---|---|
| +1, Thin Al | Aluminum $305 \pm 30Å$<br>Polyimide $1940 \pm 100Å$ | Synchrotron<br>SAO Monochromator |
| +1, Thick Al | Aluminum $1663 \pm 50Å$<br>Aluminum $305 \pm 30Å$<br>Polyimide $1940 \pm 100Å$ | SAO Monochromator |
| -1, Thin Al | Aluminum $315 \pm 30Å$<br>Polyimide $2040 \pm 100Å$ | SAO Monochromator |
| -1, Thick Al | Aluminum $315 \pm 30Å$<br>Aluminum $1710 \pm 50Å$<br>Polyimide $2040 \pm 100Å$ | Synchrotron<br>SAO Monochromator |
| 0, Thick Al | Aluminum $665 \pm 50Å$<br>Polyimide $2500 \pm 100Å$<br>Aluminum $307 \pm 30Å$ | SAO Monochromator |

Table 1: Description of the witness samples that were tested with the SAO x-ray monochromator, and at the BESSY Synchrotron Light Source Facility.

| Beam Filter | Energy range (eV) | energy step (eV) | Absorption Edge |
|---|---|---|---|
| Beryllium 0.25 $\mu m$ | 60 – 71 | 1 | |
| Beryllium 0.25 $\mu m$ | 71.2 – 75 | 0.2 | Aluminum LII,LIII |
| Beryllium 0.25 $\mu m$<br>No Filter<br>Titanium 1 $\mu m$ | 76 – 110<br>100 – 250<br>250 – 280 | 1<br>2<br>2 | |
| Titanium 1 $\mu m$ | 280.5 – 293 | 0.5 | Carbon K |
| Titanium 1 $\mu m$ | 295 – 400 | 5 | |
| Titanium 1 $\mu m$ | 400.2 – 415 | 0.2 | Nitrogen K |
| Titanium 1 $\mu m$<br>Iron 0.5 $\mu m$<br>Iron 0.5 $\mu m$ | 416 – 450<br>450 – 520<br>521 – 529 | 1<br>3<br>1 | |
| Iron 0.5 $\mu m$ | 529.2 – 540 | 0.2 | Oxygen K |
| Iron 0.5 $\mu m$<br>Iron 0.5 $\mu m$<br>Iron 0.5 $\mu m$<br>Copper 0.5 $\mu m$<br>Berylium 7 $\mu m$ | 541 – 565<br>541 – 600<br>605 – 700<br>700 – 900<br>900 – 1540 | 1<br>1<br>5<br>5<br>10 | |
| Berylium 7 $\mu m$ | 1542 – 1600 | 2 | Aluminum K |
| Berylium 7 $\mu m$<br>Berylium 7 $\mu m$ | 1605 – 1700<br>1710 – 1950 | 5<br>10 | |

Table 2: Energies surveyed in the BESSY synchrotron transmission measurements.

| Filter Segment | Al ($\mu$g/cm$^2$) | C ($\mu$g/cm$^2$) | N ($\mu$g/cm$^2$) | O ($\mu$g/cm$^2$) | Reduced $\chi^2$ |
|---|---|---|---|---|---|
| +1, Thin Al | $6.73 \pm 0.28$ | $21.08 \pm 0.74$ | $1.73 \pm 0.89$ | $7.37 \pm 0.67$ | 2.455 |
| +1, Thick Al | $47.65 \pm 0.67$ | $21.74 \pm 0.83$ | $1.79 \pm 0.96$ | $6.62 \pm 1.38$ | 3.499 |
| -1, Thin Al | $7.92 \pm 0.47$ | $21.10 \pm 0.66$ | $1.05 \pm 1.00$ | $6.62 \pm 1.25$ | 1.139 |
| -1, Thick Al | $49.55 \pm 0.89$ | $21.44 \pm 1.05$ | $2.06 \pm 1.07$ | $6.22 \pm 1.24$ | 2.989 |
| 0, Thick Al | $23.82 \pm 0.45$ | $26.33 \pm 0.71$ | $2.34 \pm 0.91$ | $9.83 \pm 1.19$ | 3.997 |

Table 3: Computed mass areal densities based on 1982 Henke coefficients for witness samples measured with the SAO x-ray monochromator. The reduced $\chi^2$ values of the data fits are included in the last column.

| Flight Filter Segment | Luxel ($\AA$) | SAO Derived Thicknesses ($\AA$) |
|---|---|---|
| +1, Thin Al | $305 \pm 30$ | $269.0 \pm 11.0$ |
| +1, Thick Al | $1968 \pm 58$ | $1906.0 \pm 26.8$ |
| -1, Thin Al | $315 \pm 30$ | $316.8 \pm 18.8$ |
| -1, Thick Al | $2025 \pm 58$ | $1980.0 \pm 35.0$ |
| 0, Thick Al | $972 \pm 58$ | $952.8 \pm 18.0$ |

Table 4: Comparison of the Luxel aluminum thickness values with the thickness values derived from the SAO x-ray monochromator data. Note that the values agree within the limits of error.

| Filter Segment | Luxel Thickness ($\AA$) | Derived Thickness ($\AA$) |
|---|---|---|
| +1, Thin Al | $1940 \pm 100$ | $2150 \pm 95$ |
| +1, Thick Al | $1940 \pm 100$ | $2150 \pm 134$ |
| -1, Thin Al | $2040 \pm 100$ | $2060 \pm 124$ |
| -1, Thick Al | $2040 \pm 100$ | $2120 \pm 140$ |
| 0, Thick Al | $2500 \pm 100$ | $2750 \pm 118$ |

Table 5: The derived polymide thicknesses for the witness samples are compared against Luxel's measured values. The thicknesses are derived from the SAO monochromator data. The hydrogen areal density was not incorporated into the derived values, as it makes a negligible contribution to the polyimide areal density.

| Filter Segment | Al ($\mu$g/cm$^2$) | C ($\mu$g/cm$^2$) | N ($\mu$g/cm$^2$) | O ($\mu$g/cm$^2$) | Test Method |
|---|---|---|---|---|---|
| +1, Thin Al | $7.26 \pm 0.16$ | $20.94 \pm 0.62$ | $1.68 \pm 0.52$ | $7.11 \pm 0.40$ | Synchrotron |
| +1, Thick Al | $47.65 \pm 0.67$ | $21.74 \pm 0.83$ | $1.79 \pm 0.96$ | $6.62 \pm 1.38$ | SAO Monochromator |
| -1, Thin Al | $7.92 \pm 0.47$ | $21.10 \pm 0.66$ | $1.05 \pm 1.00$ | $6.62 \pm 1.25$ | SAO Monochromator |
| -1, Thick Al | $50.34 \pm 0.45$ | $20.00 \pm 0.93$ | $1.84 \pm 0.75$ | $7.54 \pm 0.45$ | Synchrotron |

Table 6: The mass areal densities from the best fit results of the x-ray synchrotron transmission measurements, compared to the SAO monochromator results obtained in differing aluminum thickness regions.

| Filter Segment Pairing | Ratio of Al Mass Areal Densities | Ratio of Luxel Al Thickness values |
|---|---|---|
| +1, Thick Al<br>+1, Thin Al | $6.56 \pm 0.17$ | $6.45 \pm 0.69$ |
| -1, Thick Al<br>-1, Thin Al | $6.36 \pm 0.38$ | $6.43 \pm 0.66$ |

Table 7: A comparison of the ratio of Al mass areal densities of two pairs of witness samples with the ratio of the aluminum thickness values measured by Luxel. Note that the results agree within the limits of error.

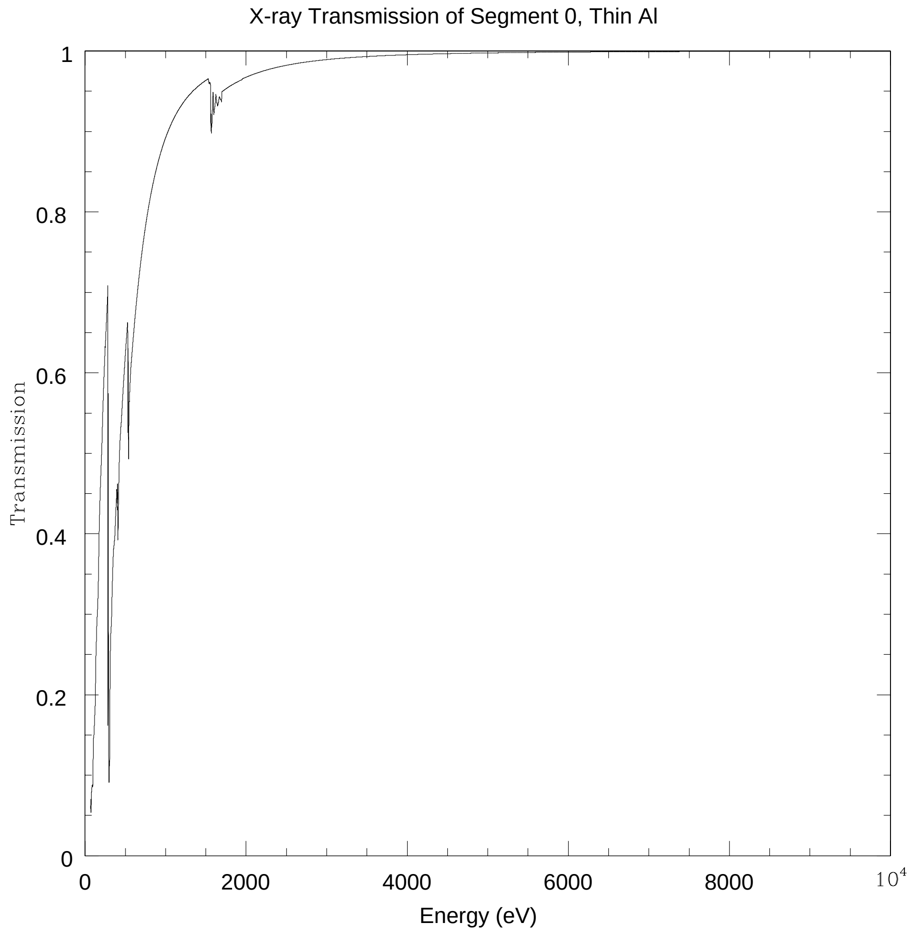


Figure 4: The flight UVIS-S x-ray transmission model in the thin aluminum region of segment 0 is shown over the 0 to 10,000eV energy range. Because synchrotron measurements were not obtained on a representative witness sample, the above model for energies at and below 1950 eV was determined from: x-ray transmission measurements of the thick Al region of segment 0; the difference in nominal aluminum thickness of this segment; the nominal density of deposited aluminum; and the 1982 Henke coefficients. Above 1950 eV, the model is based upon measurements obtained with the SAO x-ray monochromator.

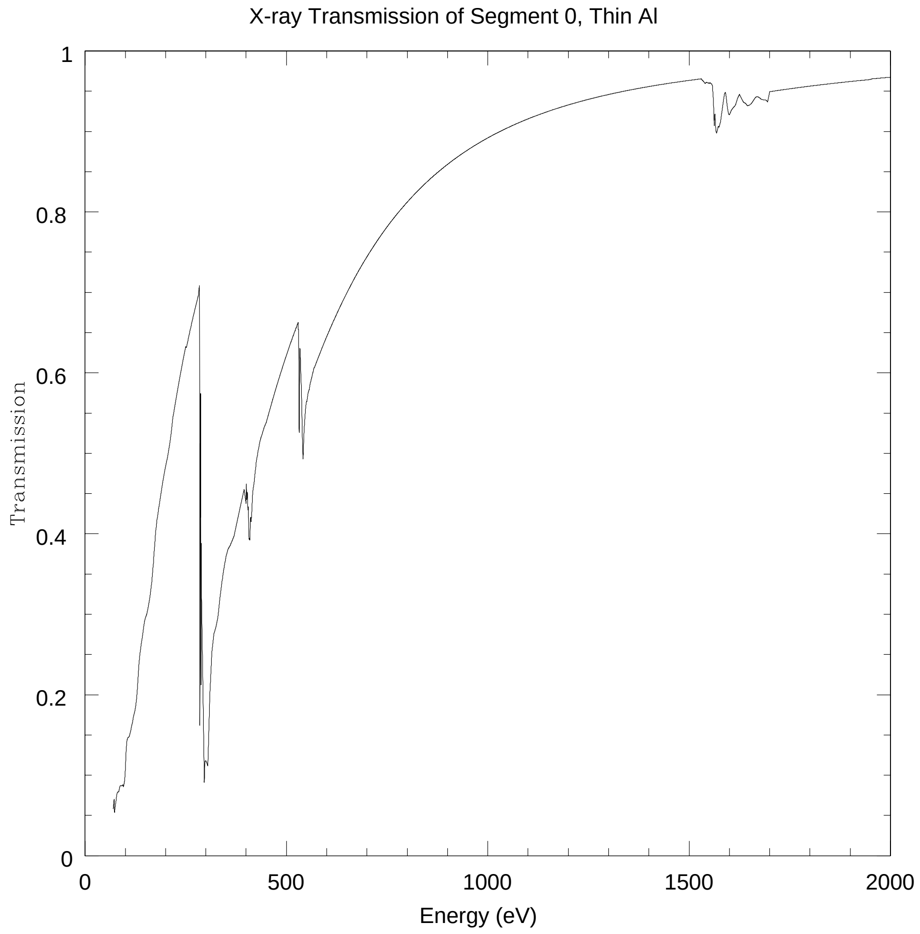


Figure 5: This is a plot of the above model, but displayed over the 0 to 2,000eV energy range. Since the x-ray transmission of a witness sample for this filter segment was never measured, there are no data points to go with this figure.

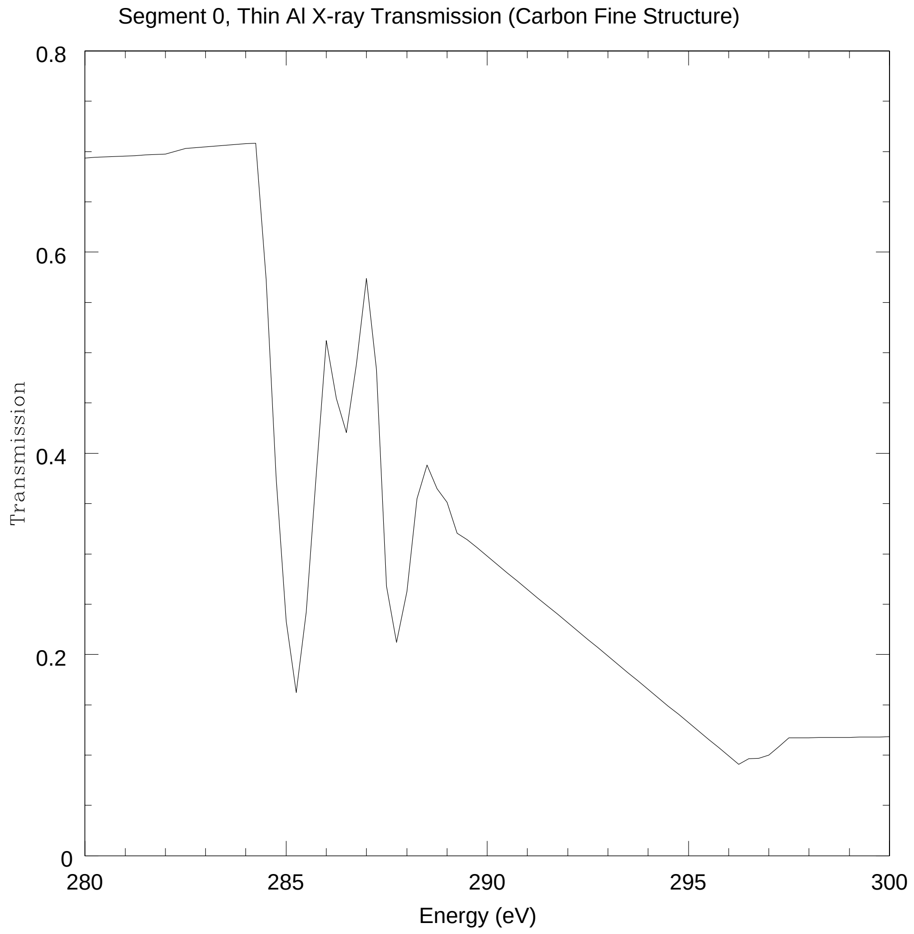


Figure 6: The flight UVIS-S x-ray transmission model in the carbon K-edge fine structure region for the thin Al section of segment 0. Since the x-ray transmission of a witness sample for this filter segment was never measured, there are no data points to go with this figure.

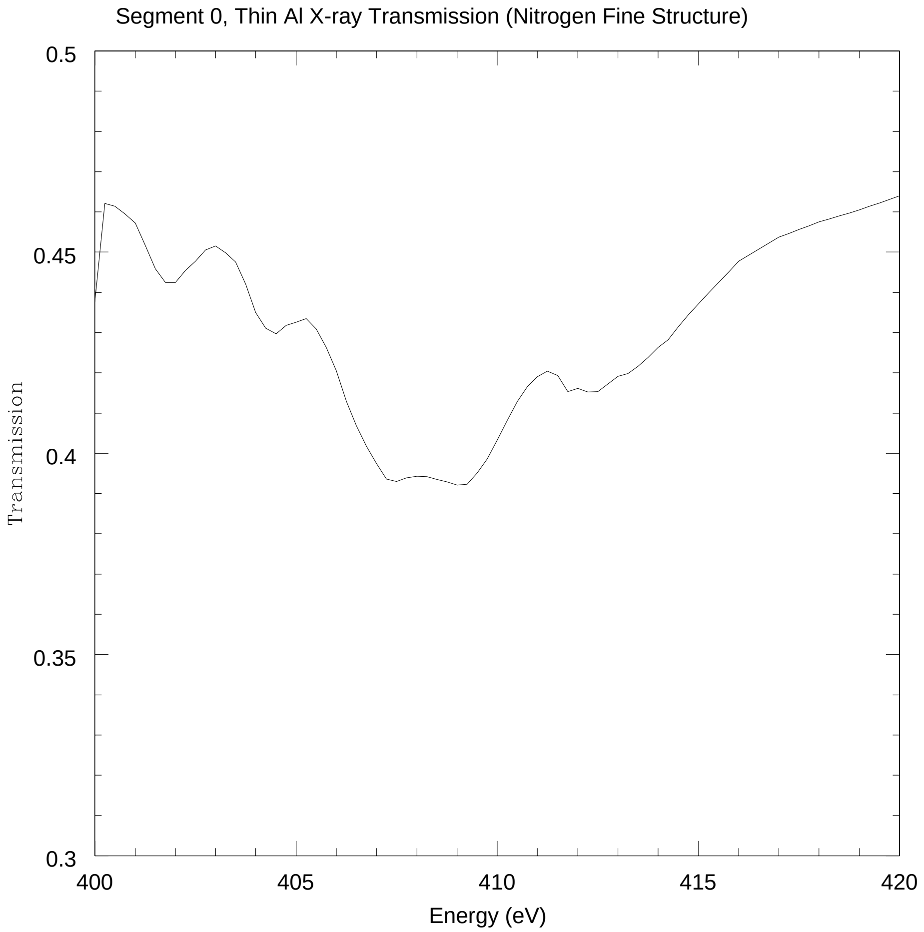


Figure 7: The flight UVIS-S x-ray transmission model in the nitrogen K-edge fine structure region for the thin Al section of segment 0. Since the x-ray transmission of a witness sample for this filter segment was never measured, there are no data points to go with this figure.

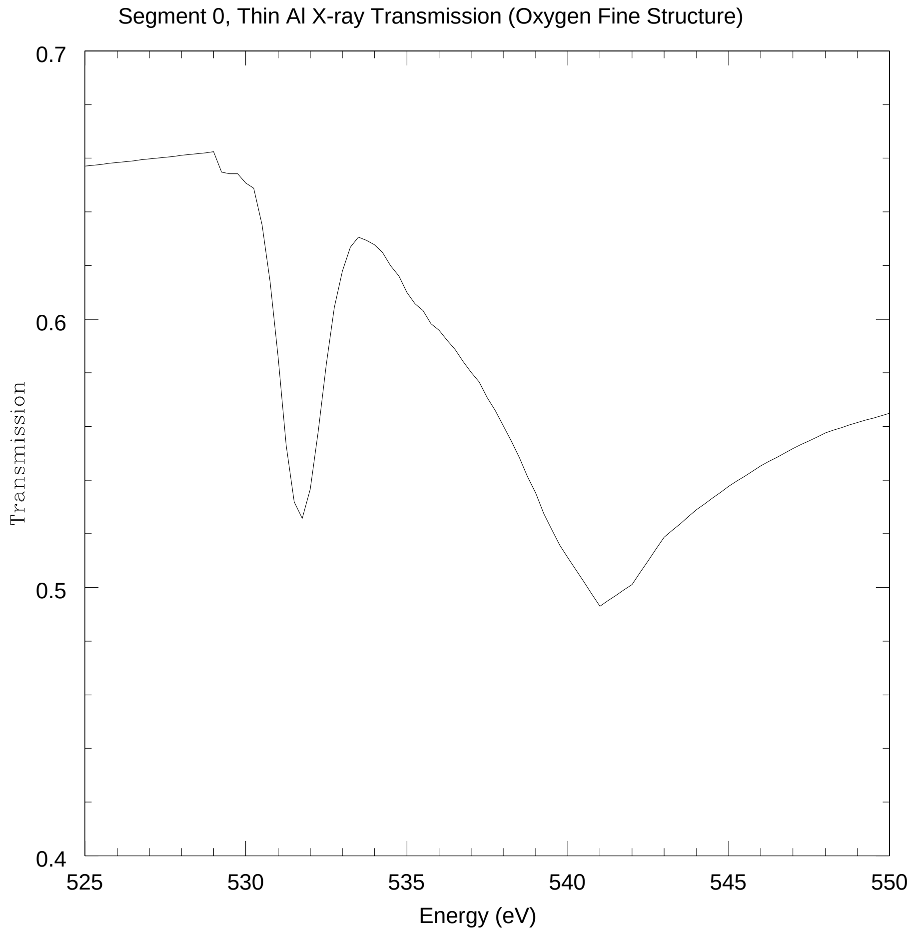


Figure 8: The flight UVIS-S x-ray transmission model in the oxygen K-edge fine structure region for the thin Al section of segment 0. Since the x-ray transmission of a witness sample for this filter segment was never measured, there are no data points to go with this figure.

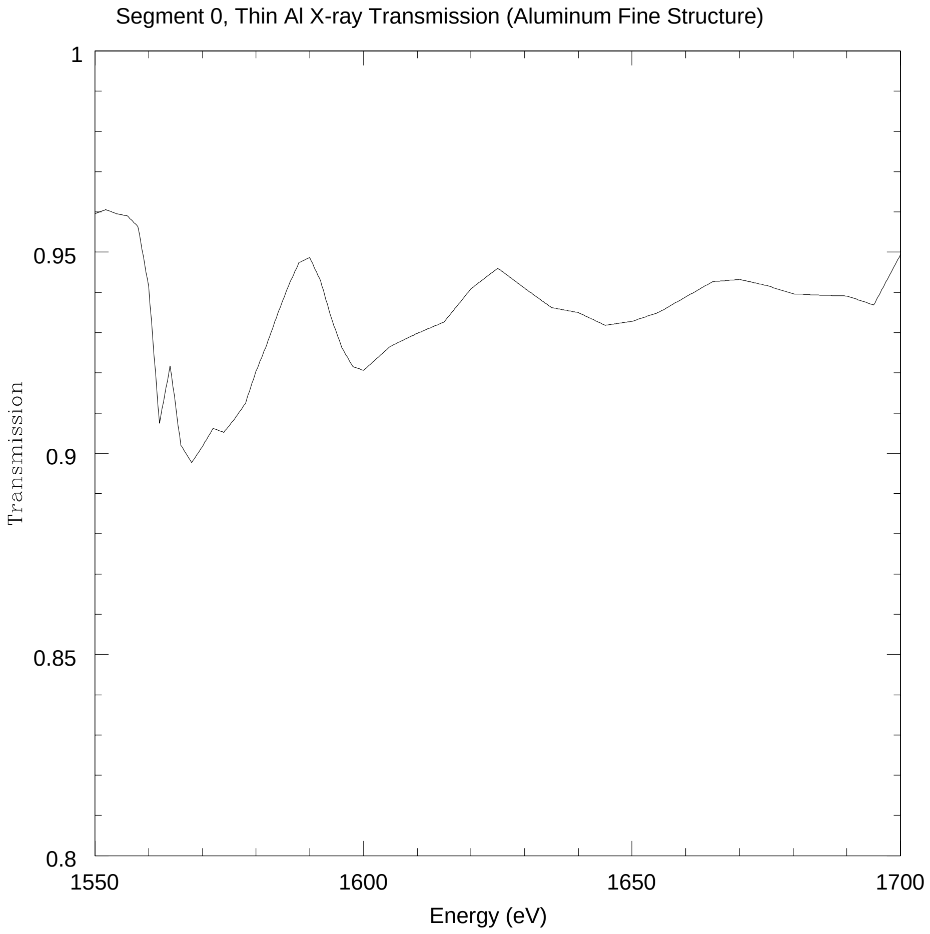


Figure 9: The flight UVIS-S x-ray transmission model in the aluminum K-edge fine structure region for the thin Al section of segment 0. Since the x-ray transmission of a witness sample for this filter segment was never measured, there are no data points to go with this figure.

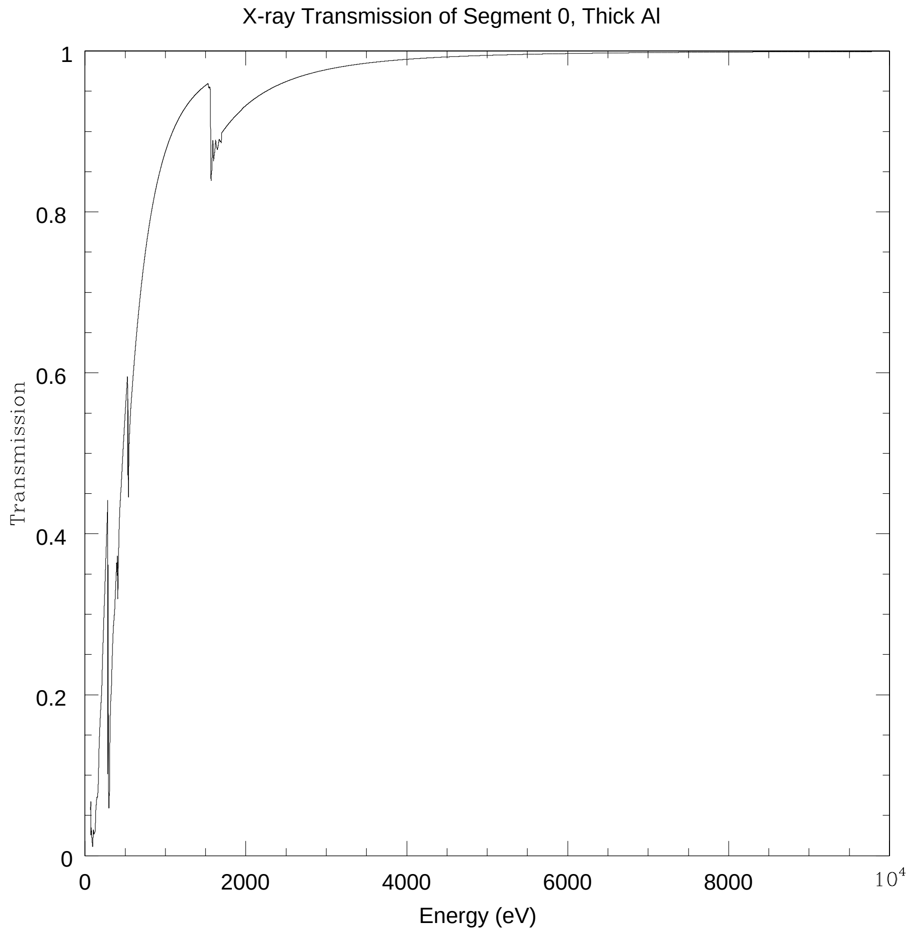


Figure 10: The flight UVIS-S x-ray transmission model in the thick aluminum region of segment 0 is shown over the 0 to 10,000eV energy range. It is the result of combining the model based upon the BESSY synchrotron data (out to 1950 eV) with the SAO monochromator model.

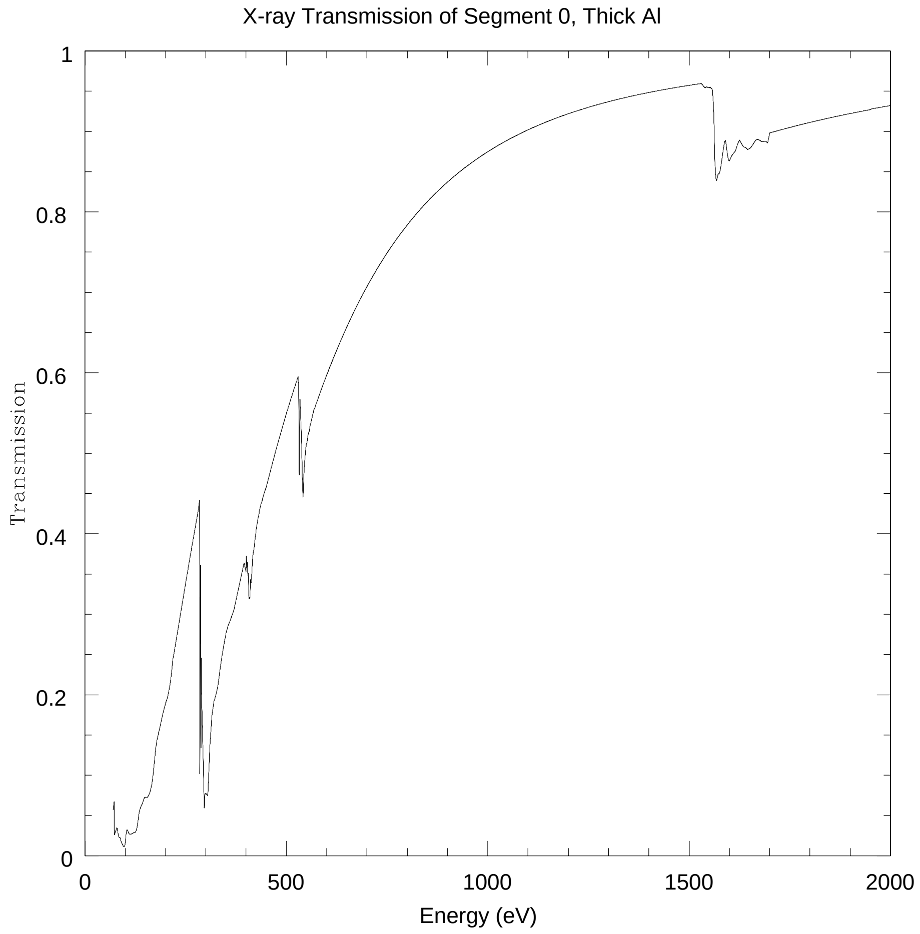


Figure 11: This is a plot of the above model, but displayed over the 0 to 2,000eV energy range.

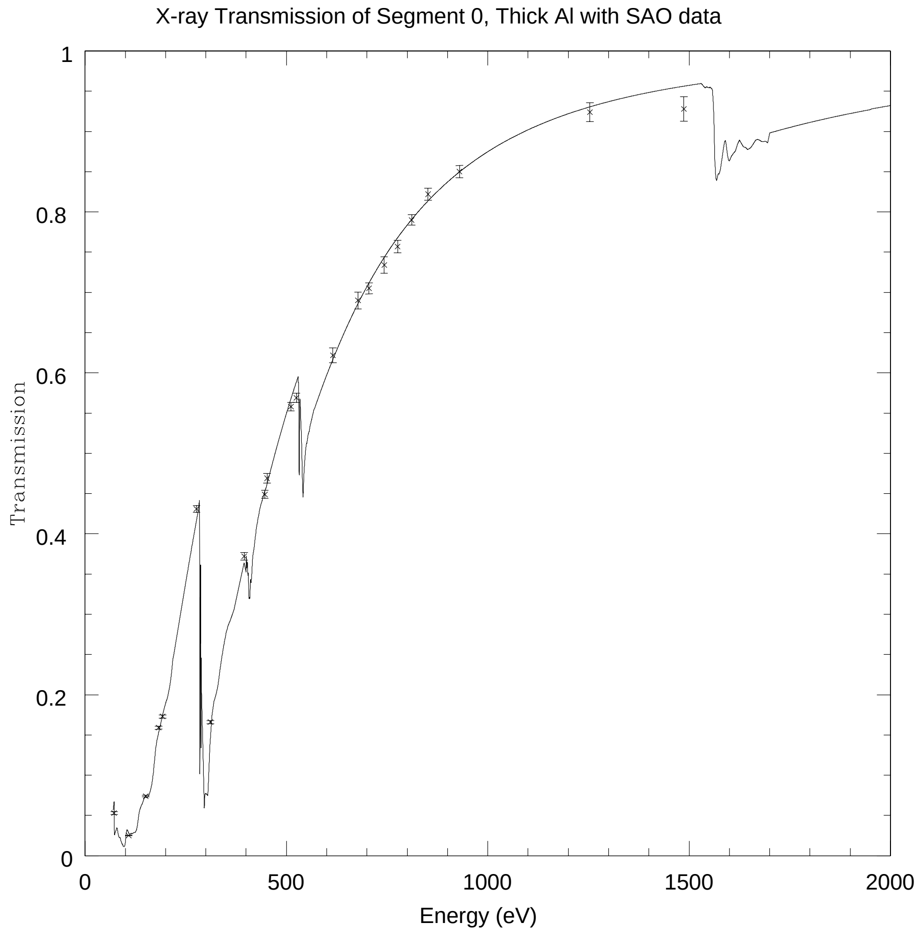


Figure 12: This is a plot of the x-ray transmission in the thick aluminum region of segment 0 over the 0 to 2keV energy regime. Included in this plot are the tranmsission measurements obtained on a witness sample using the SAO x-ray monochromator.

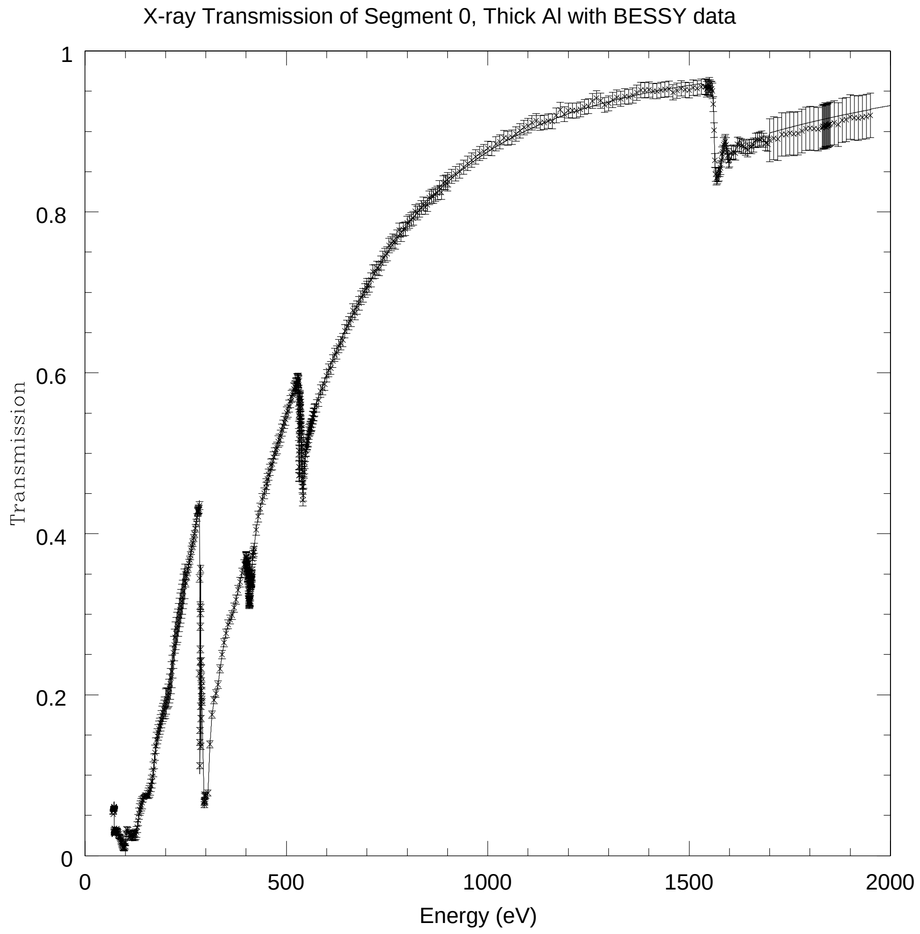


Figure 13: This is a plot of the x-ray transmission in the thick aluminum region of segment 0 over the 0 to 2keV energy regime. Included in this plot are the tranmsission measurements obtained on a witness sample using the BESSY synchrotron facility.

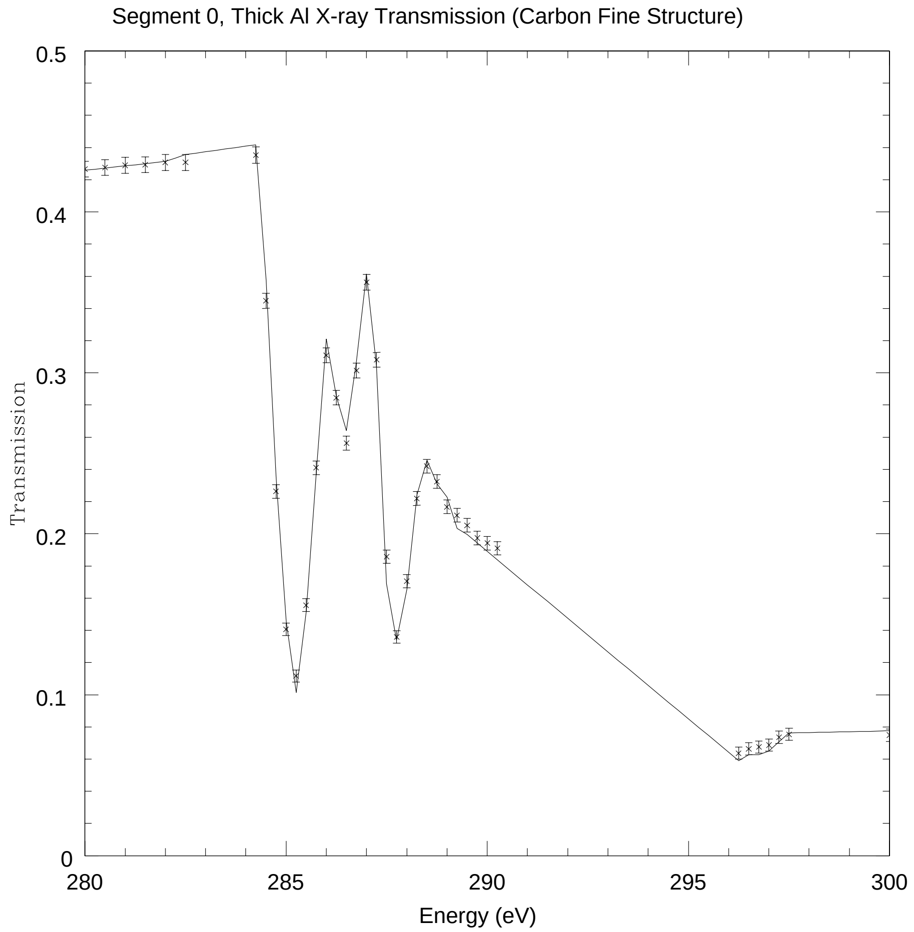


Figure 14: The flight UVIS-S x-ray transmission model in the carbon K-edge fine structure region. The model in this region (segment 0, thick aluminum) is based upon the x-ray transmission data (shown above) obtained on a witness sample using the BESSY synchrotron.

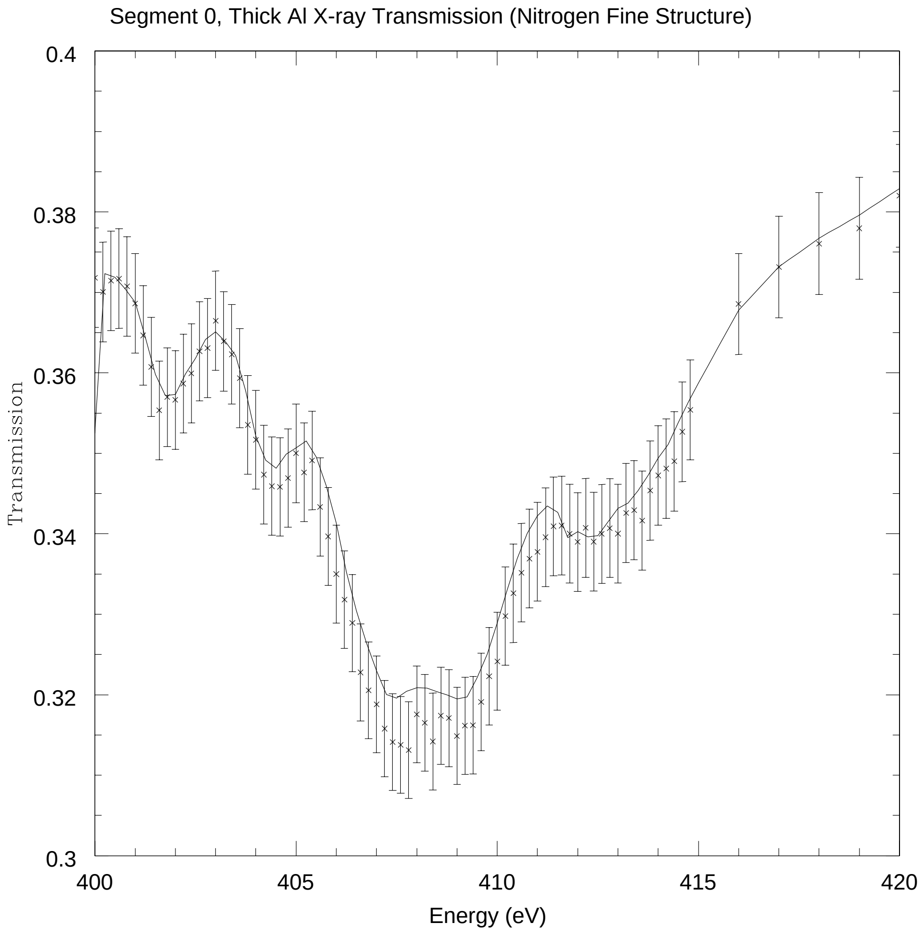


Figure 15: The flight UVIS-S x-ray transmission model in the nitrogen K-edge fine structure region. The model in this region (segment 0, thick aluminum) is based upon the x-ray transmission data (shown above) obtained on a witness sample using the BESSY synchrotron.

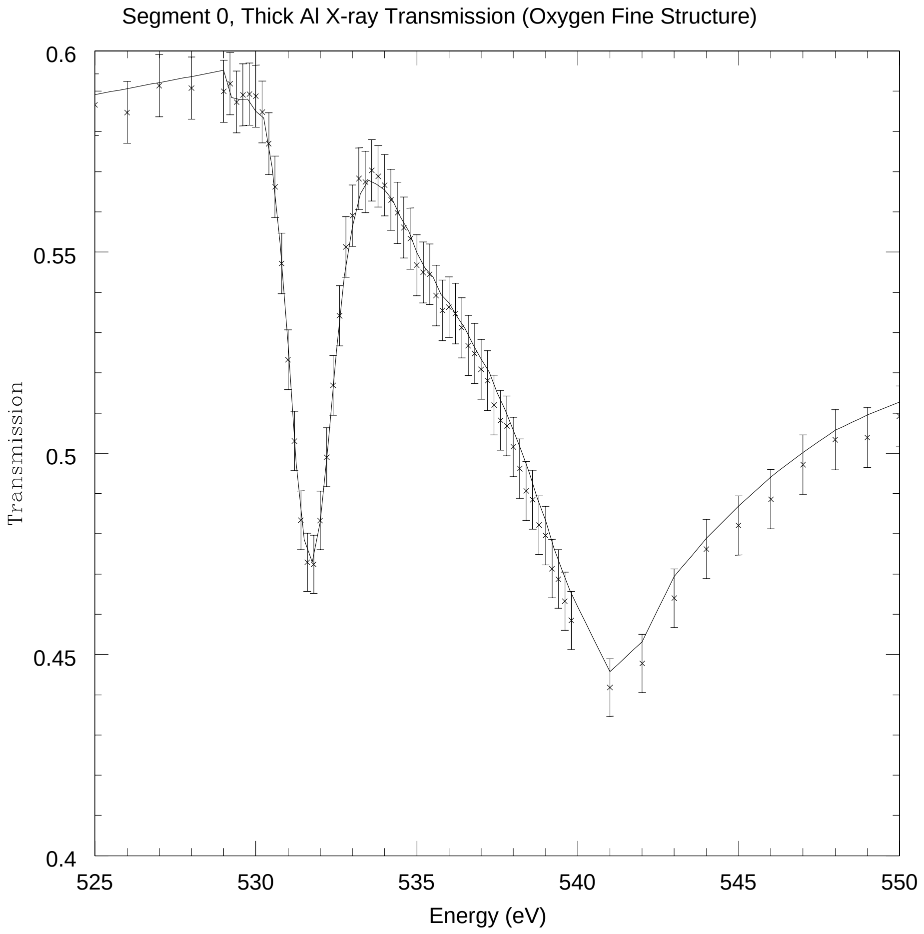


Figure 16: The flight UVIS-S x-ray transmission model in the oxygen K-edge fine structure region. The model in this region (segment 0, thick aluminum) is based upon the x-ray transmission data (shown above) obtained on a witness sample using the BESSY synchrotron.

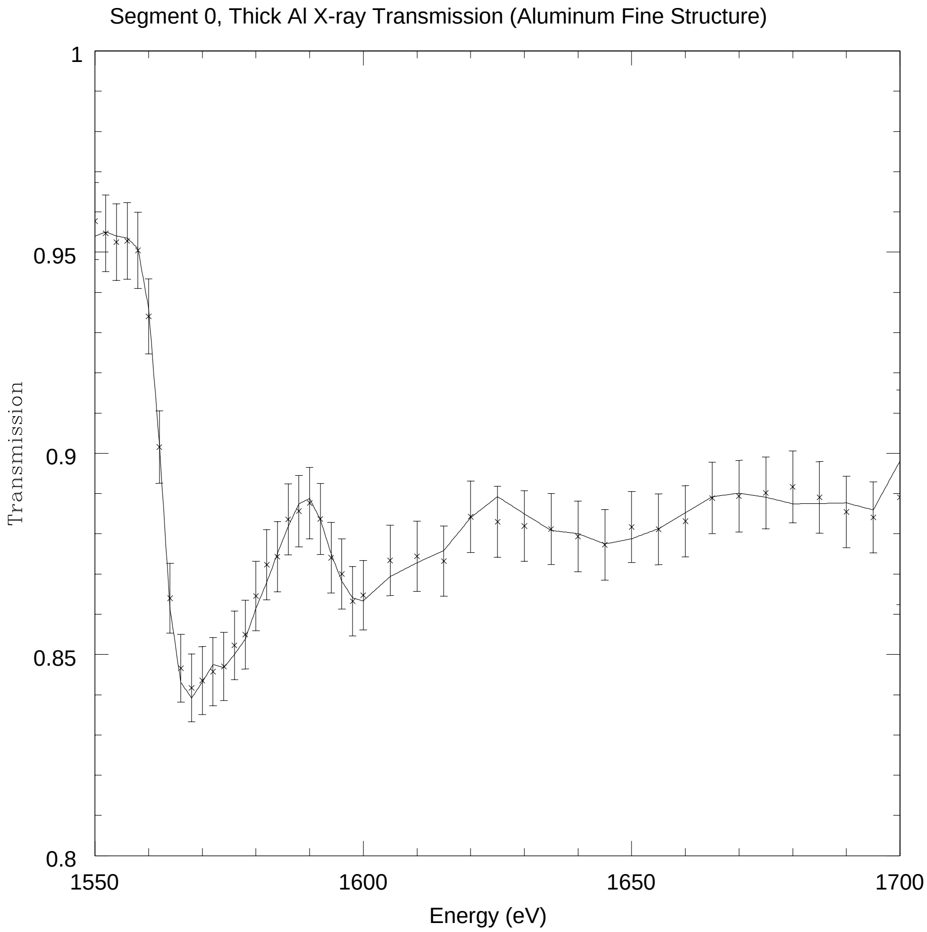


Figure 17: The flight UVIS-S x-ray transmission model in the aluminum K-edge fine structure region. The model in this region (segment 0, thick aluminum) is based upon the x-ray transmission data (shown above) obtained on a witness sample using the BESSY synchrotron.

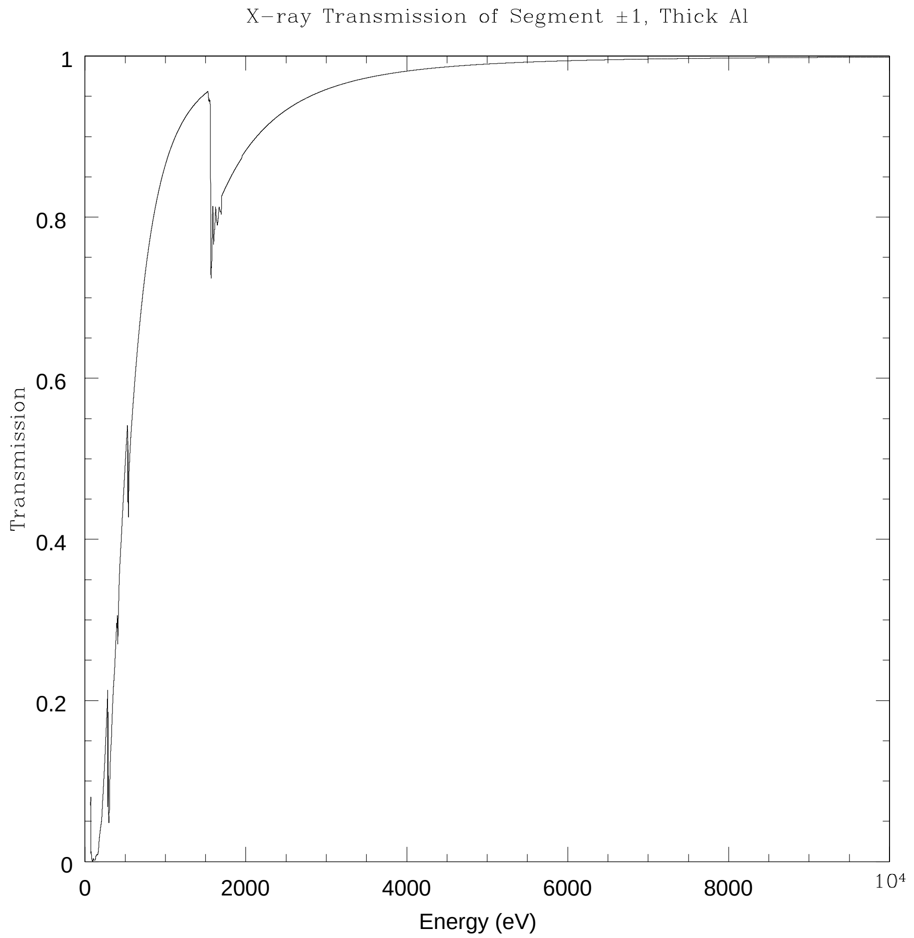


Figure 18: The flight UVIS-S x-ray transmission model in the thick aluminum region of the ±1 segments is shown over the 0 to 10,000eV energy range. It is the result of combining the model based upon the BESSY synchrotron data (out to 1950 eV) with the SAO monochromator model.

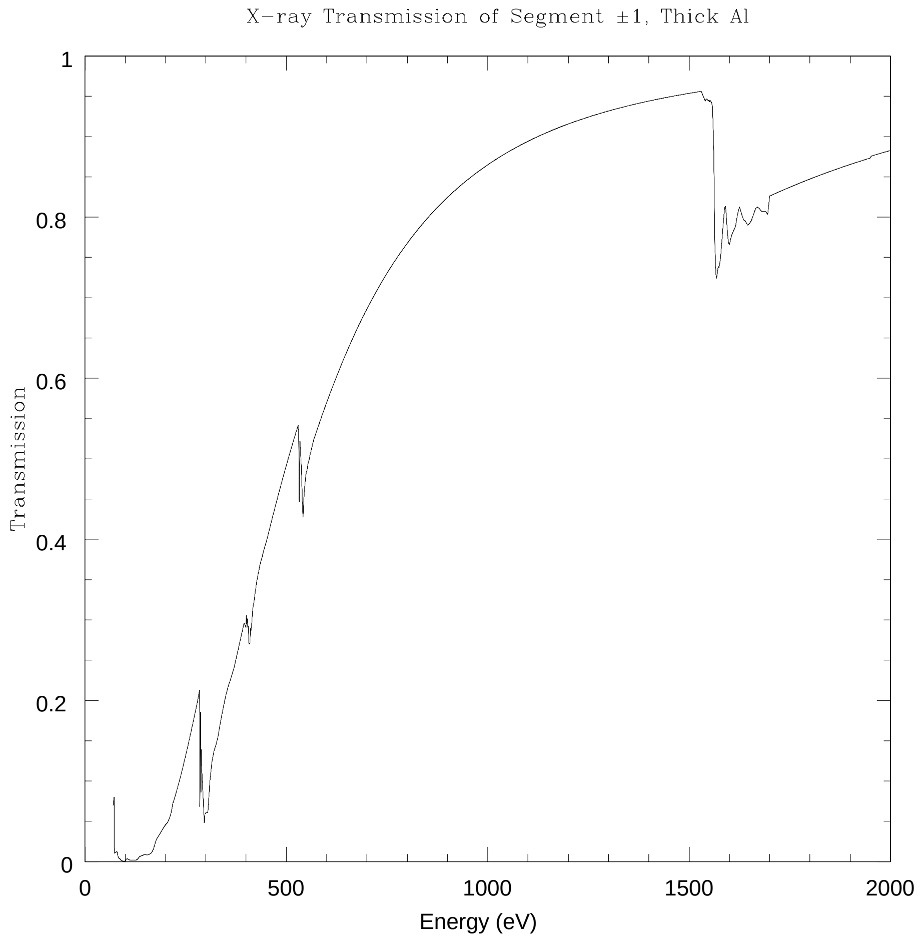


Figure 19: This is a plot of the above model, but displayed over the 0 to 2,000eV energy range.

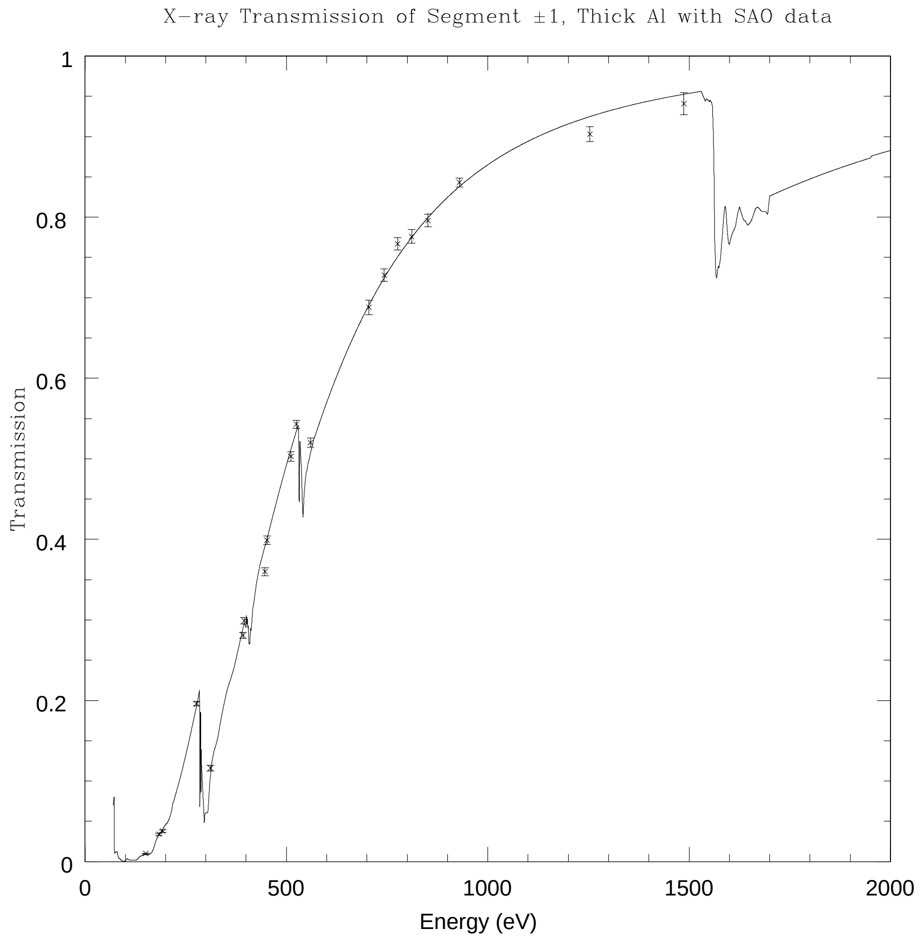


Figure 20: This is a plot of the x-ray transmission in the thick aluminum region of the $\pm 1$ segments over the 0 to 2keV energy regime. Included in this plot are the tranmsission measurements obtained on a witness sample using with the SAO x-ray monochromator.

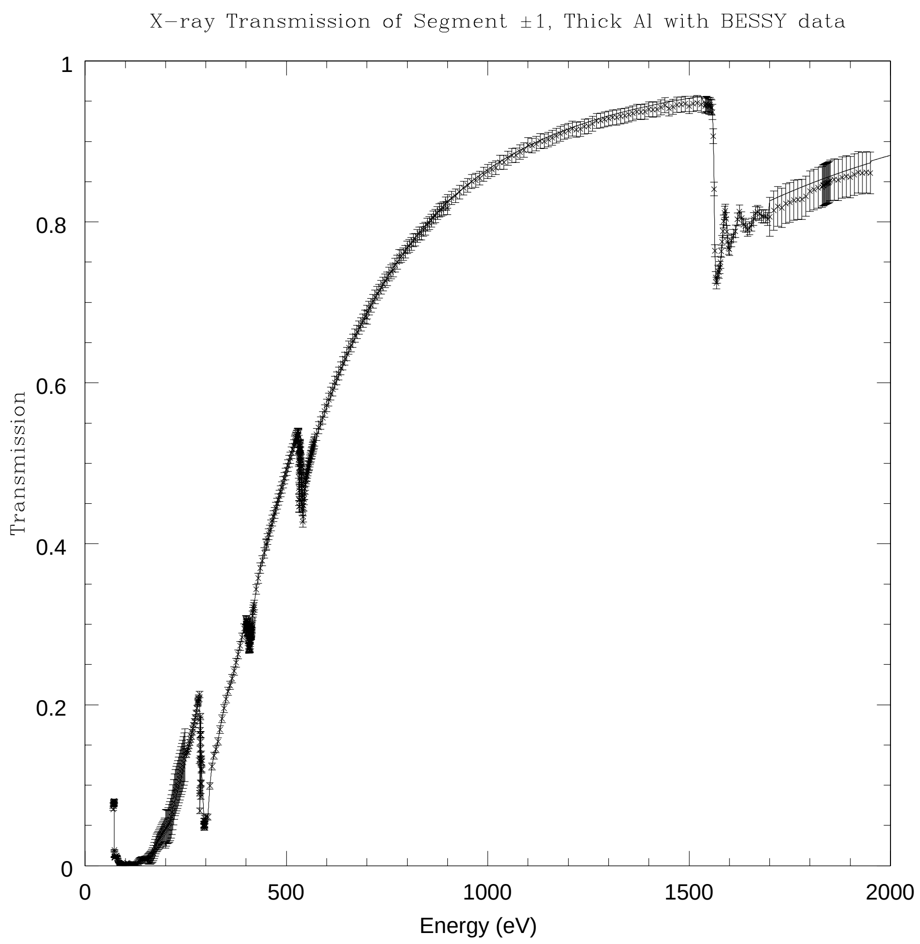


Figure 21: This is a plot of the x-ray transmission in the thick aluminum region of the ±1 segments over the 0 to 2keV energy regime. Included in this plot are the tranmsission measurements obtained on a witness sample using the BESSY synchrotron facility.

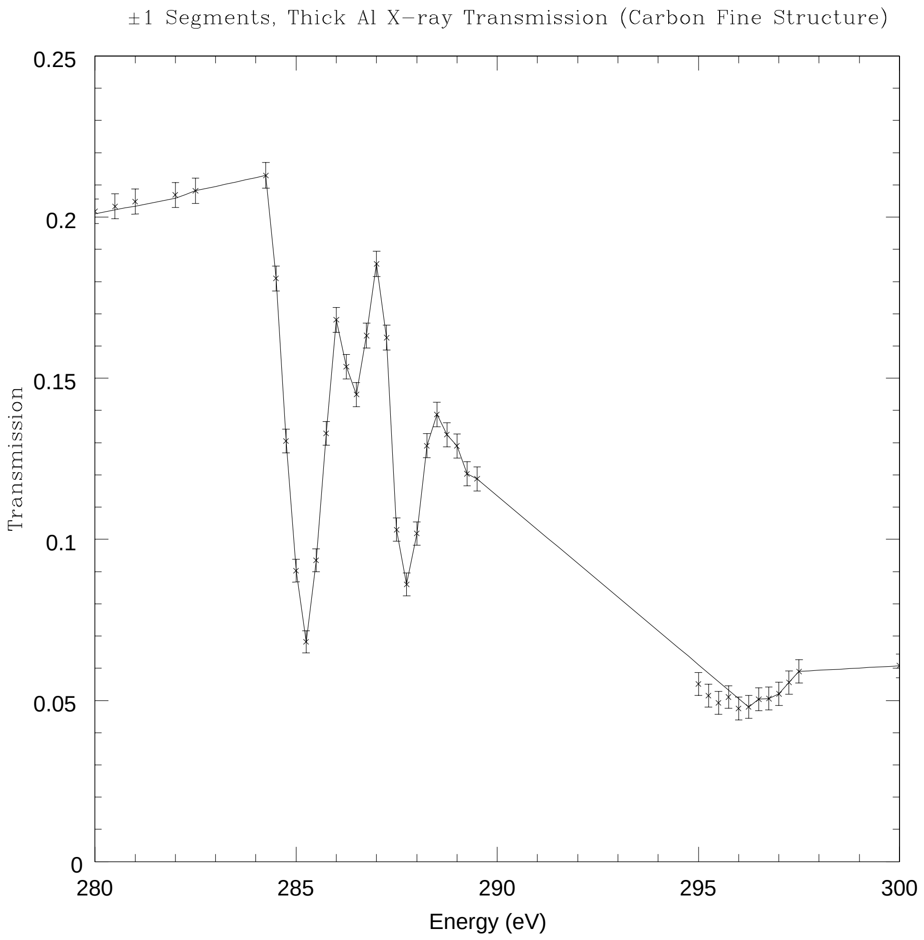


Figure 22: The flight UVIS-S x-ray transmission model in the carbon K-edge fine structure region. The model in this region (±1 segment, thick aluminum) is based upon the x-ray transmission data (shown above) obtained on a witness sample using the BESSY synchrotron.

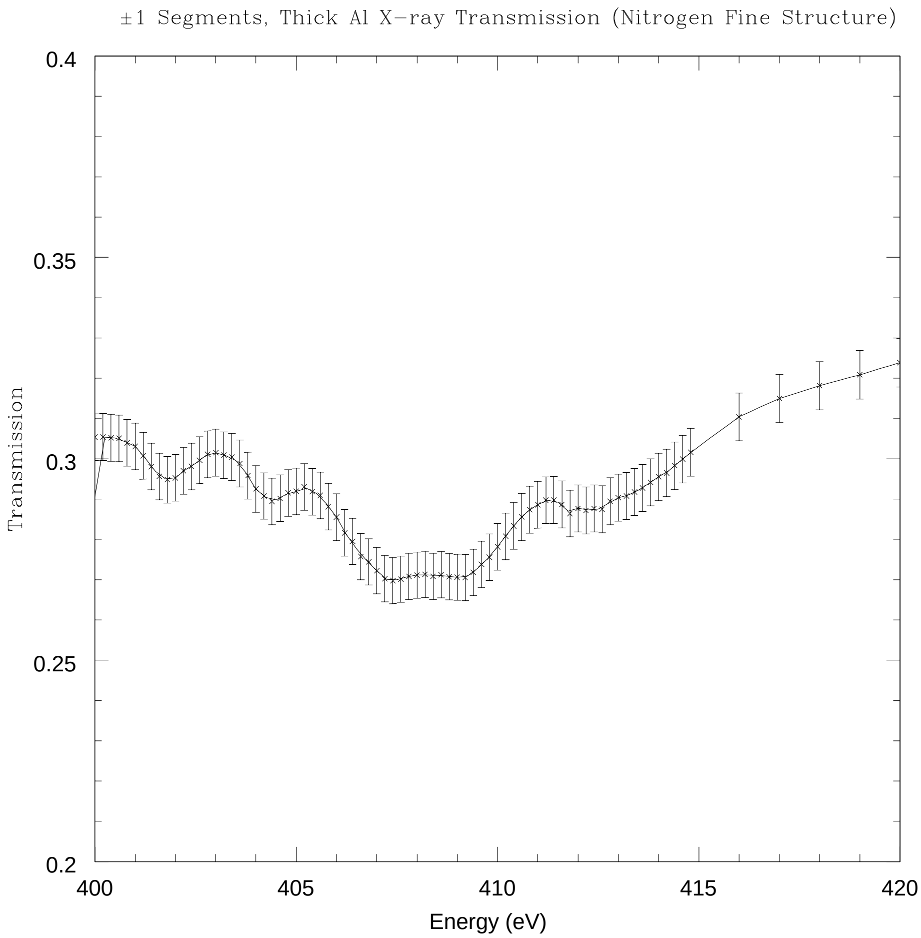


Figure 23: The flight UVIS-S x-ray transmission model in the nitrogen K-edge fine structure region. The model in this region (±1 segment, thick aluminum) is based upon the x-ray transmission data (shown above) obtained on a witness sample using the BESSY synchrotron.

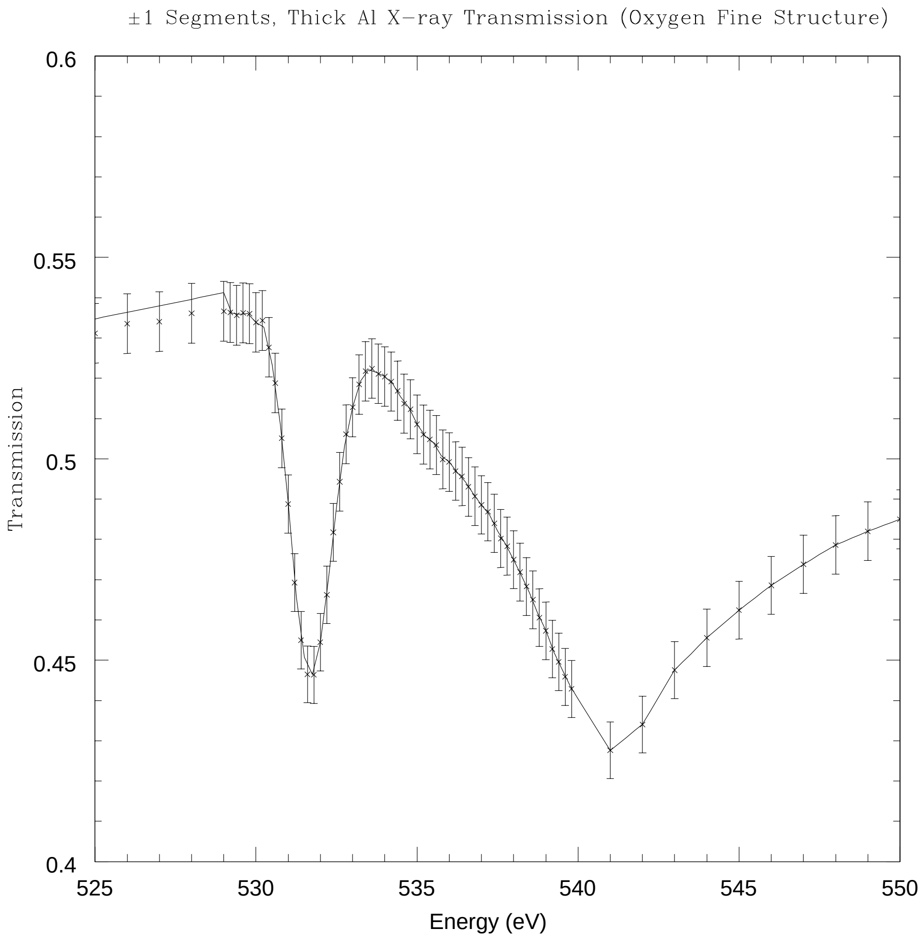


Figure 24: The flight UVIS-S x-ray transmission model in the oxygen K-edge fine structure region. The model in this region (±1 segment, thick aluminum) is based upon the x-ray transmission data (shown above) obtained on a witness sample using the BESSY synchrotron.

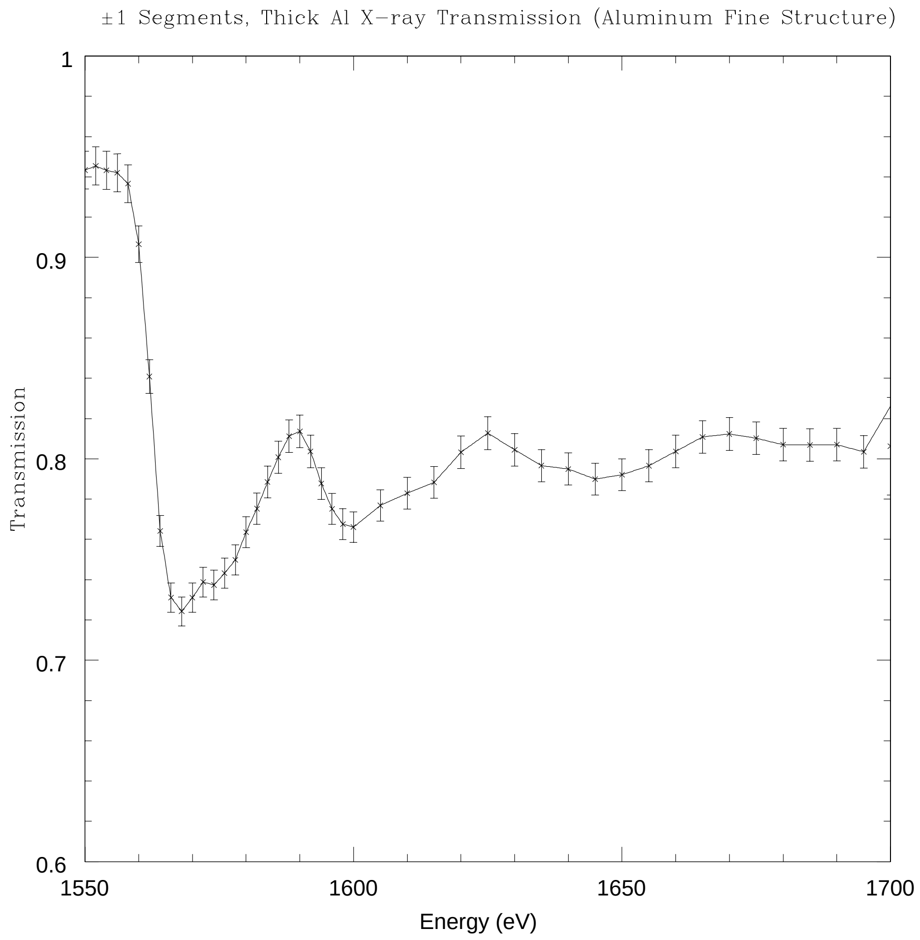


Figure 25: The flight UVIS-S x-ray transmission model in the aluminum K-edge fine structure region. The model in this region (±1 segment, thick aluminum) is based upon the x-ray transmission data (shown above) obtained on a witness sample using the BESSY synchrotron.

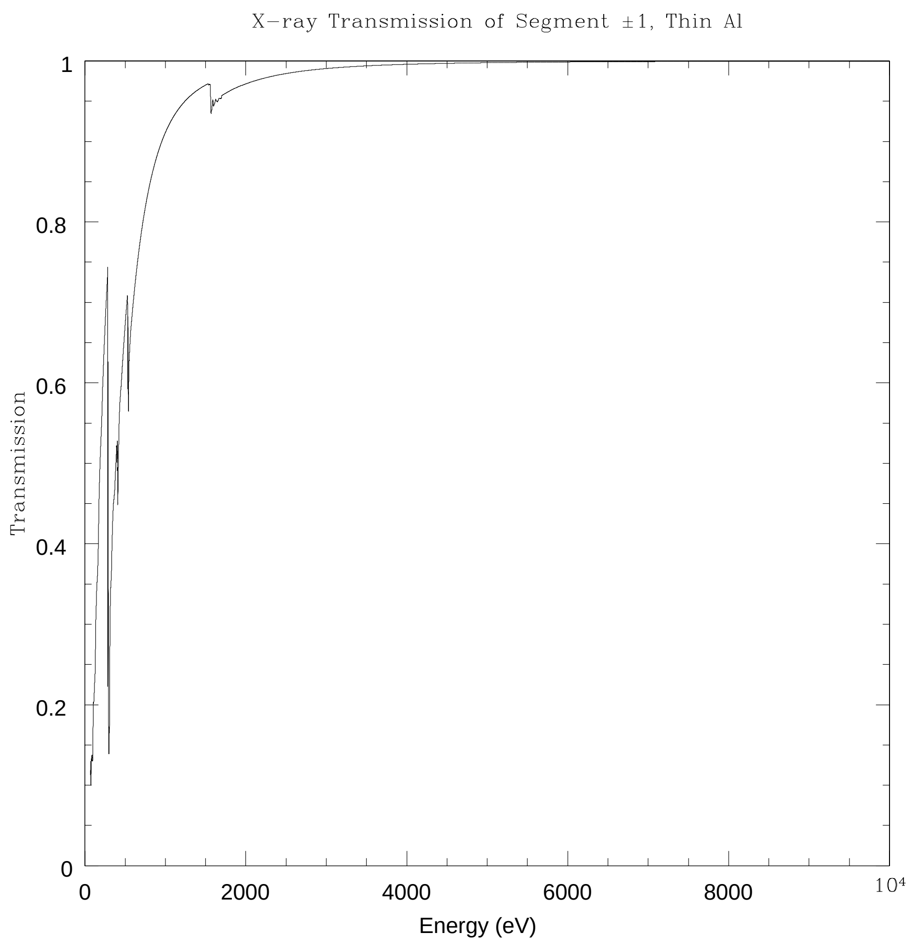


Figure 26: The flight UVIS-S x-ray transmission model in the thin aluminum region of the filter's ±1 segments is shown over the 0 to 10,000eV energy range. Because synchrotron measurements of witness samples in the thin Al region of the −1 segment were not obtained, the transmission was calculated from measurements of the witness sample representing the thick aluminum region of the −1 segment, the known mass absorption coefficients, and the aluminum thicknesses (both thin and thick regions) as provided by Luxel.

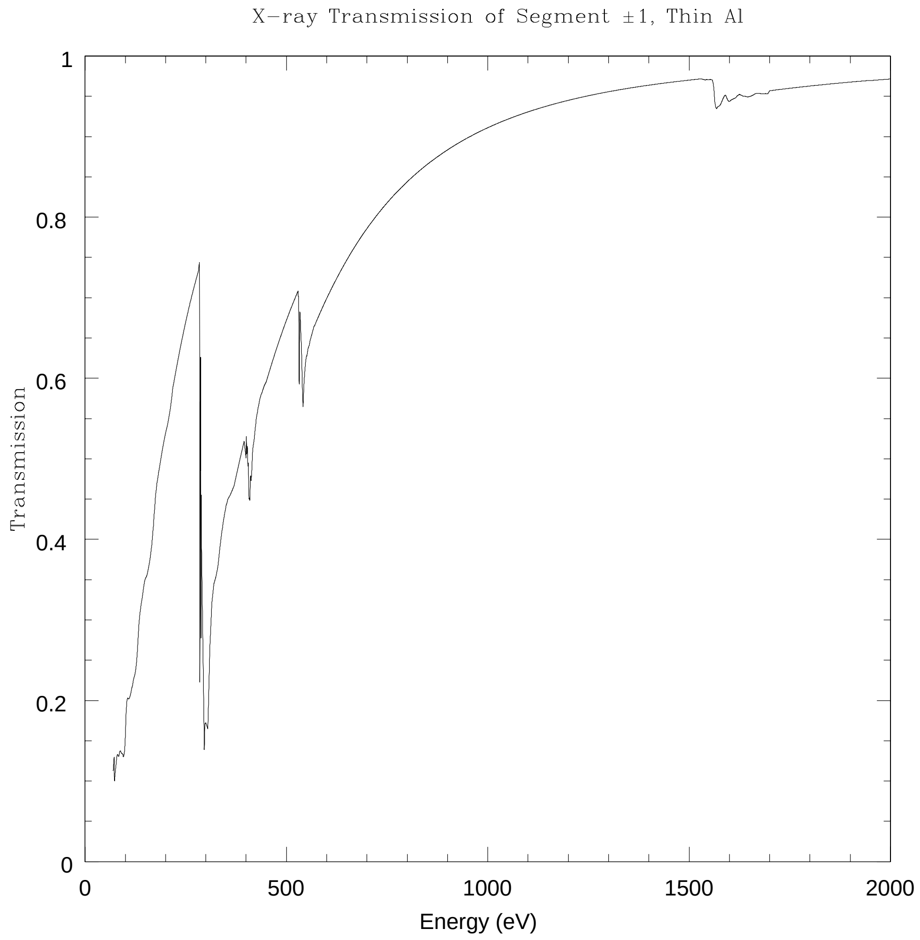


Figure 27: This is a plot of the above model, but displayed over the 0 to 2,000eV energy range.

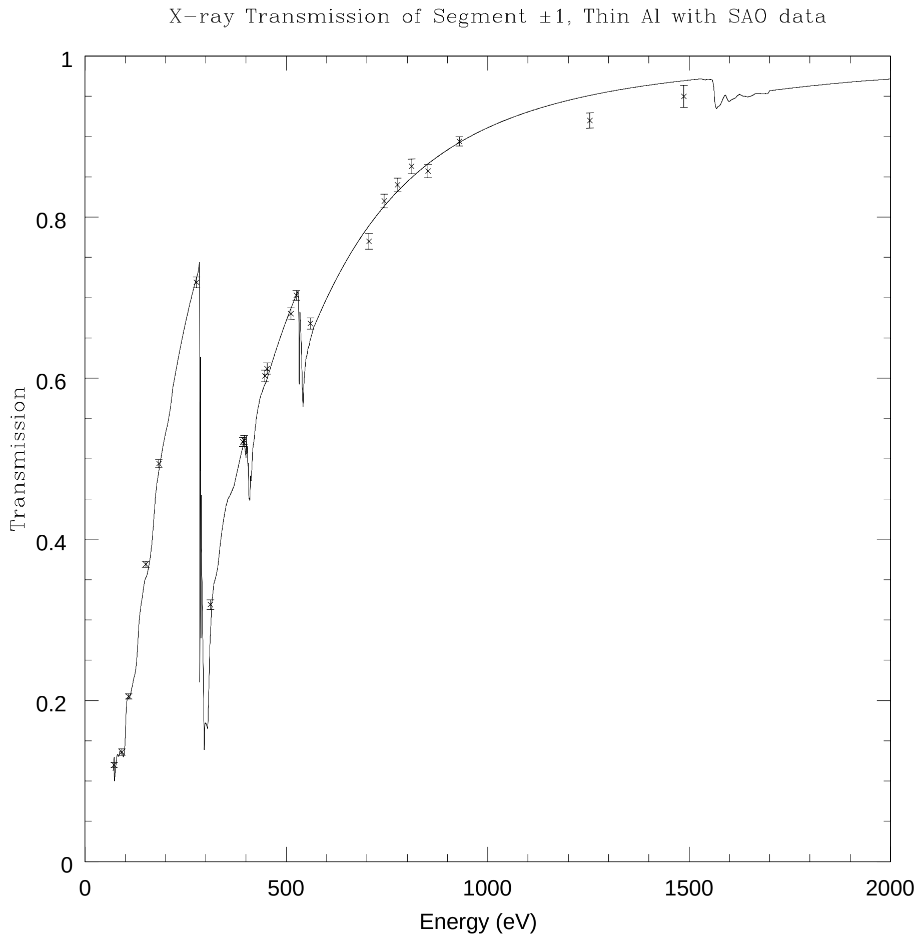


Figure 28: This is a plot of the x-ray transmission in the thin aluminum region of the $\pm 1$ segments over the 0 to 2keV energy regime. Included in this plot are the tranmsission measurements obtained with the SAO x-ray monochromator.

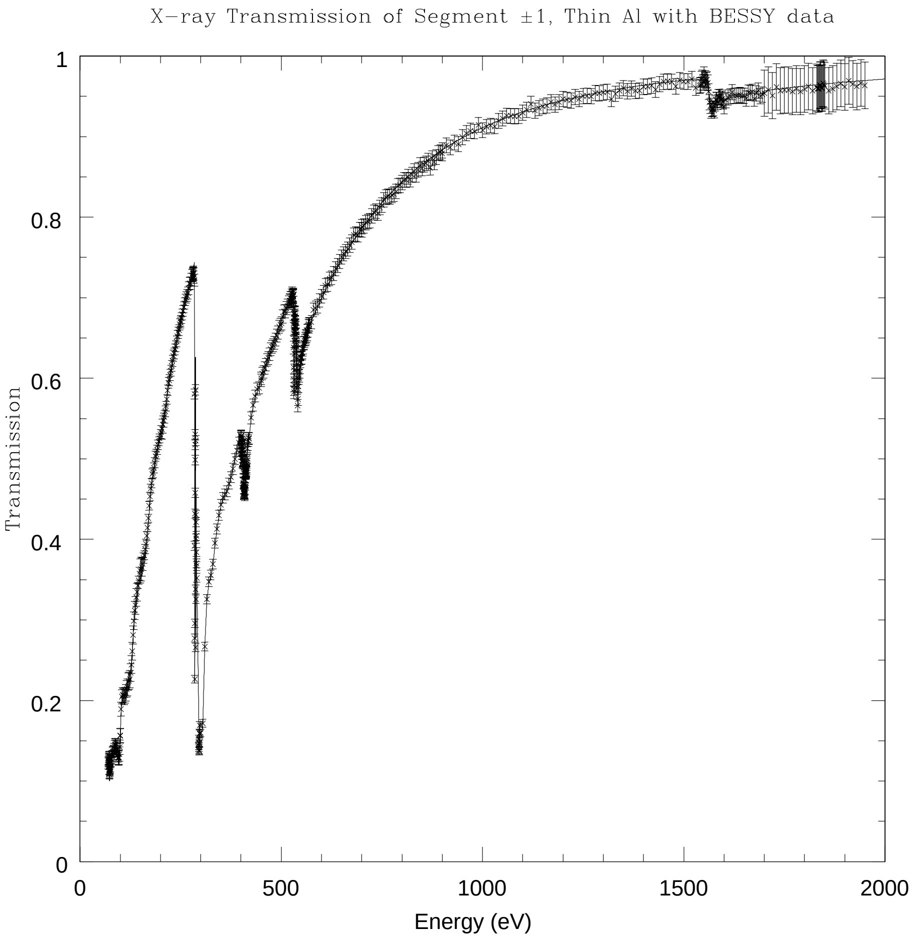


Figure 29: This is a plot of the x-ray transmission in the thin aluminum region of the $\pm 1$ segments over the 0 to 2keV energy regime. Included in this plot are the tranmsission measurements obtained at the BESSY synchrotron facility.

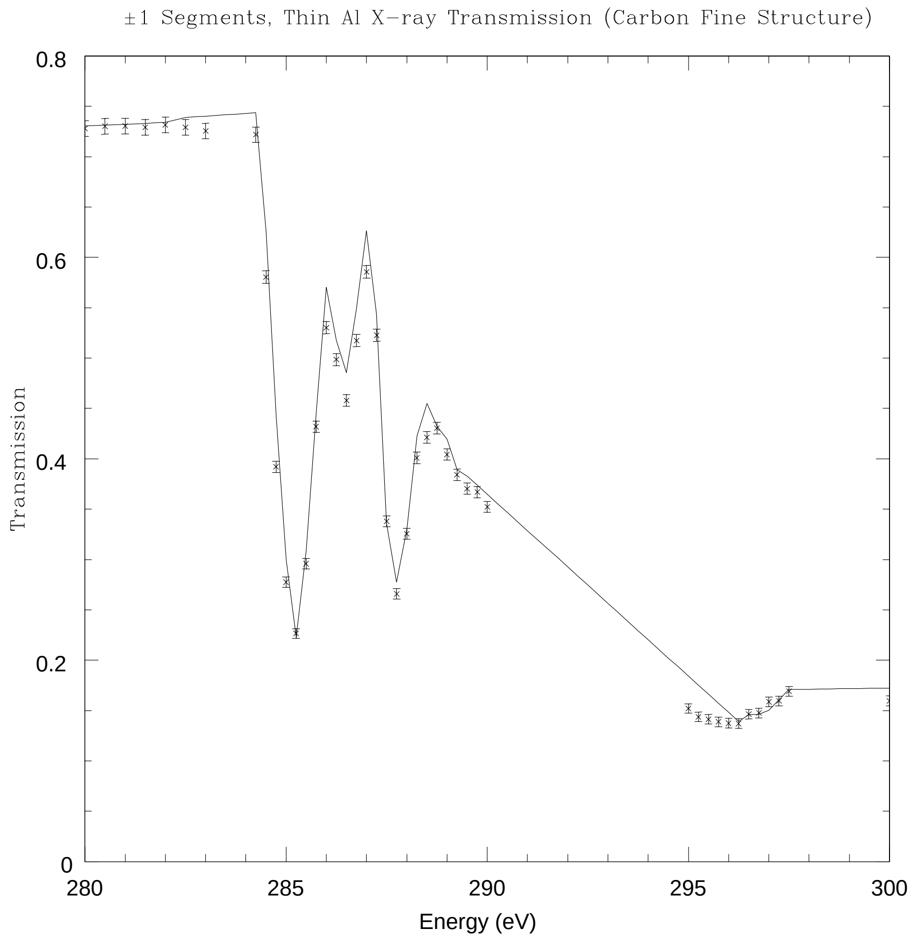


Figure 30: The flight UVIS-S x-ray transmission model in the carbon K-edge fine structure region for the $\pm1$ segment, thin aluminum. The data points represent synchrotron measurements obtained on a witness sample associated with the thin Al region of the $+1$ segment.

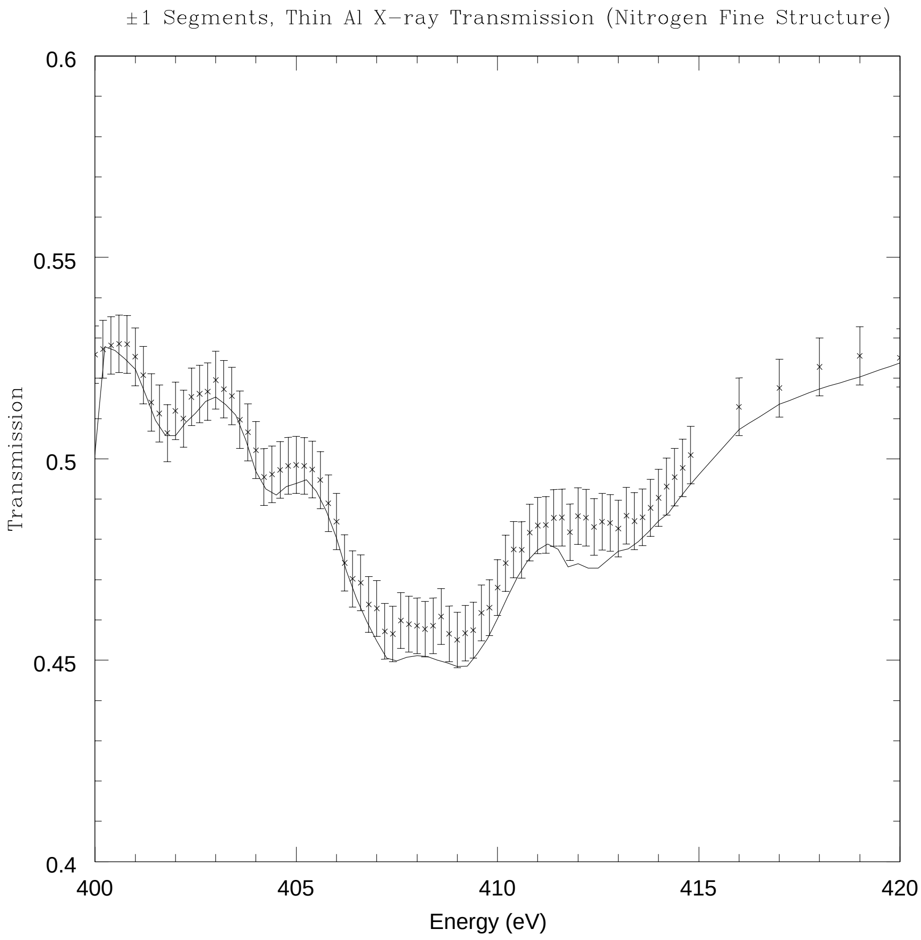


Figure 31: The flight UVIS-S x-ray transmission model in the nitrogen K-edge fine structure region for the ±1 segment, thin aluminum. The data points represent synchrotron measurements obtained on a witness sample associated with the thin Al region of the +1 segment.

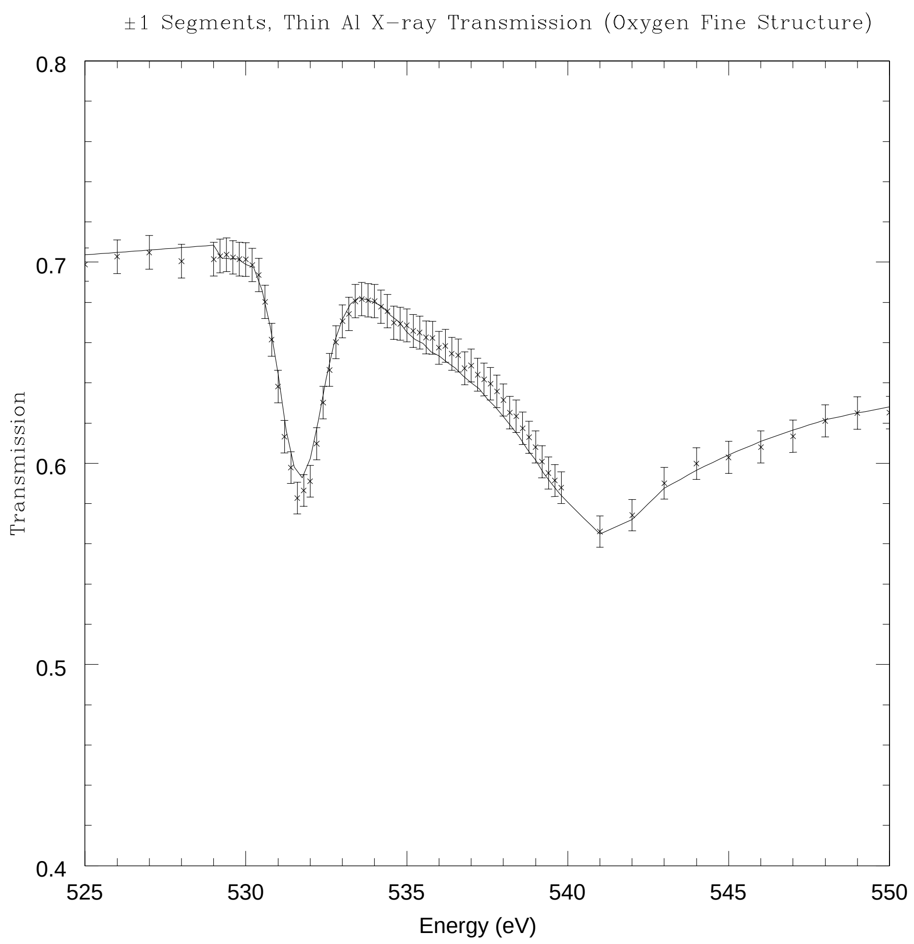


Figure 32: The flight UVIS-S x-ray transmission model in the oxygen K-edge fine structure region for the $\pm 1$ segment, thin aluminum. The data points represent synchrotron measurements obtained on a witness sample associated with the thin Al region of the $+1$ segment.

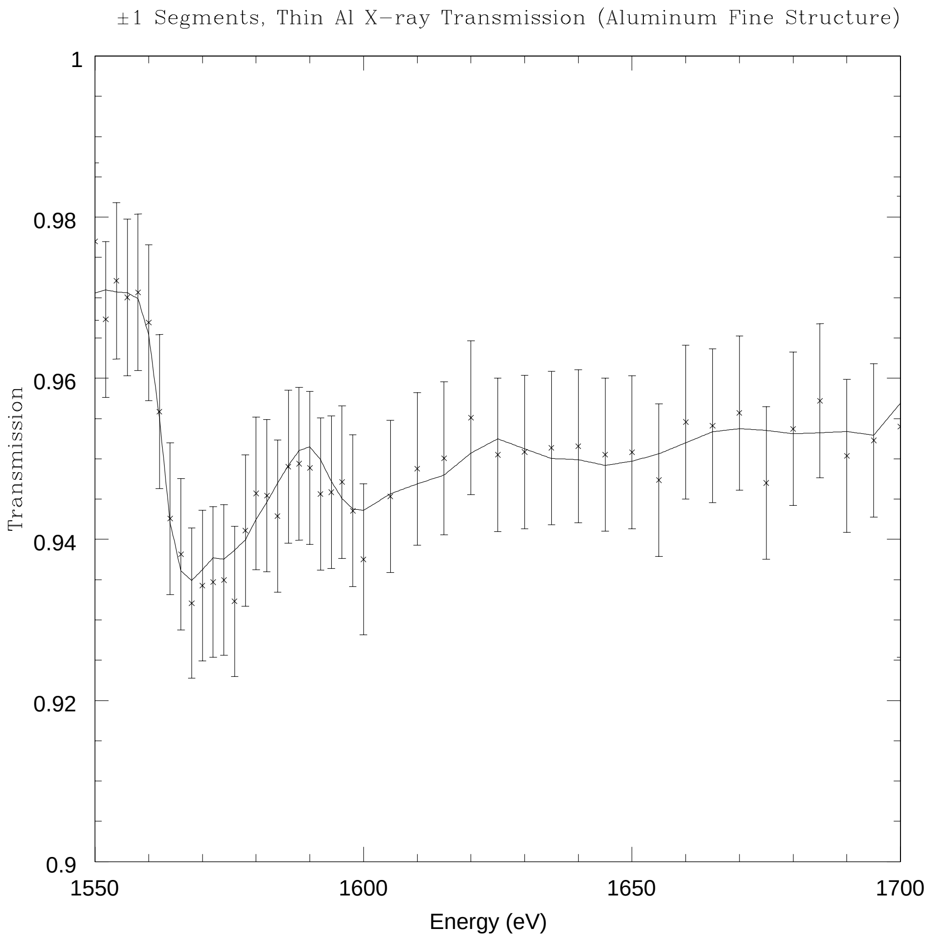


Figure 33: The flight UVIS-S x-ray transmission model in the aluminum K-edge fine structure region for the ±1 segment, thin aluminum. The data points represent synchrotron measurements obtained on a witness sample associated with the thin Al region of the +1 segment.